ISSN 0252-1075
Contribution from IITM
Research Report No. RR-130

Development of Extended Range Prediction System Using CFSv2 and Its Verification

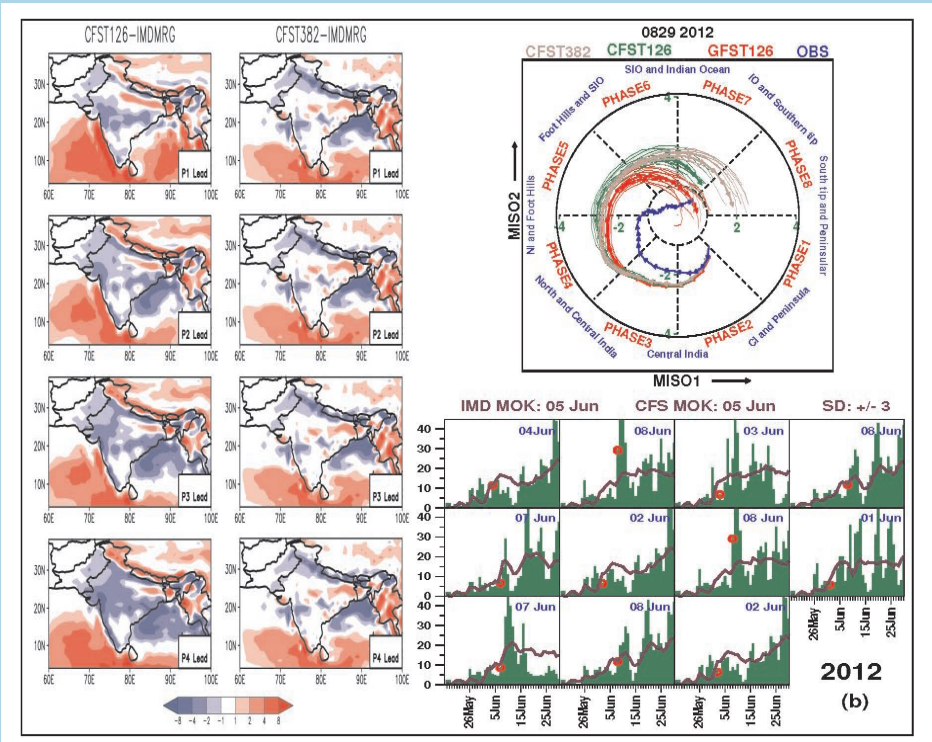

N. Borah, S. Abhilash, S. Joseph, R. Chattopadhyay, S. Sharmila and A.K. Sahai

July 2013

Indian Institute of Tropical Meteorology
Pune - 411 008, India

Development of Extended Range Prediction System Using CFSv2 and Its verification

N. Borah, S. Abhilash, S. Joseph, R. Chattopadhyay,

S. Sharmila and A.K. Sahai

July 2013

Indian Institute of Tropical Meteorology

Dr. Homi Bhabha Road, Pashan Pune - 411 008

Maharashtra, India

E-mail : lip@tropmet.res.in Fax : 91-020-25865142

Web : http://www.tropmet.res.in Telephone : 91-020-25904200

CONTENTS

ABSTRACT

An ensemble prediction system (EPS) has been adopted to generate a large number of forecasts of Indian summer monsoon rainfall (ISMR) in an extended range scale from different initial conditions using the state-of-the-art NCEP Climate Forecast System Version 2 (CFSv2) model. The EPS is developed to conform with the growing need of probabilistic forecast than the deterministic one. This will add more decision-making capabilities to the user community in practical sense by providing the expected spreads or uncertainties in terms of probability from the forecast. The EPS produces 11 member ensemble forecasts for 25 days lead time at every 5day interval starting from 16th May to 28th September during 2001-2012. Study has been carried out over 4 different homogeneous regions of India where ISMR is more or less homogeneous. The selected regions are Central India (CEI), North-East India (NEI), North-West India (NWI), South peninsula (SPI) and a broader region, monsoon core zone of India (MZI). This report will document the developmental aspects of the EPS, its general real-time prediction performance during 2011, 2012 monsoon seasons and the skill statistics for the three category probabilistic prediction namely above normal, near normal and below normal during the last 12 years. To reduce the impact of high frequency fluctuatuions on daily scale the extended range prediction (ERP) skill of the EPS are evaluated at pentad mean scale. In addition to this, some aspects of large-scale monsoon intraseasonal oscillations, error growth statistics and the forecast of onset over Kerala are also evaluated during this period. The impact of high resolution is studied by running the model at T382 (~38km) resolution and the results are compared with that of the T126 and the atmospheric component of the same i.e. Global Forecast System model Version 2 (GFSv2) forced with the bias-corrected sst from CFS (GFSbc). CFST126 shows a considerable dry bias over the Indian landmass. Though the climatological bias in precipitation is removed considerably in T382 run, this improvement is not translated to the ERP in real-time.

1. INTRODUCTION

The long range forecast of the seasonal mean Indian summer monsoon rainfall (ISMR) is important for the policy makers [Xavier and Goswami 2007, Gadgil and Gadgil 2006] as the country's economy is greatly dependent on it. Nevertheless, it may not be very useful and meaningful when the mean rainfall is close to normal. It is well known that, 70% of the time Indian monsoon is normal. Hence, prediction of a normal all India rainfall may have a comfort factor, but not so useful for agricultural planning. Therefore, in addition to the seasonal mean all India rainfall, we need to predict some aspects of monsoon in sub-seasonal scale also. The sub-seasonal or extended range prediction (ERP) refers to a meteorological forecast more than 10 days in advance which is the normal predictability range of weather systems. It is well known that ISMR is punctuated by the spells of heavy rainfall and periods of quiescent rainfall activity, termed as 'active' and 'break' spells respectively, which contribute to the sub-seasonal or intraseasonal variability (ISV) of ISM. ERP of active/break spells of ISMR has a variety of applications depending on the user community ranging from agriculture to disaster and water management and planning. Prediction of ISM on this time scale is a challenging task, as this time scale falls between the normal predictability limit of deterministic forecast of weather phenomena and the seasonal mean. Moreover, the extended range time scale is too long to store atmospheric memory and too short to have considerable influence from oceanic variability. However, the extended range predictability arises from Monsoon Intraseasonal Oscillations (MISOs) which are the quasi-periodic northward propagating large-scale convective cloud bands that manifest as the active/break spells, as described earlier.

Importance of ERP has been recognized by the Ministry of Earth Sciences, Government of India and it has emphasized on the development of an ensemble system for dynamical Extended Range Prediction of Active/Break Spells (ERPAS) of ISMR under the National Monsoon Mission program. ERPAS group at IITM has been providing experimental real-time

forecast of the active-break spells of ISMR since 2011 up to 4 pentad lead using an indigenously developed ensemble prediction system (EPS) based on the Climate Forecast System Version 2 (CFSv2) model. The EPS generates a large number of forecasts from different initial conditions so that the expected forecast and also the expected spreads or uncertainties in terms of probability from this forecast can be informed to the user community. Such estimations of uncertainties will add more decision-making capabilities to the user community in practical sense.

Sahai et al. [2013a] and Sharmila et al. [2013] have established that the representation of MISOs in coupled general circulation model (CGCM) is more reasonable compared to atmospheric general circulation models (AGCM) due to the more realistic local SST–rainfall lag–lead relationship in CGCM. Experiment has been performed with CFST126 and the atmospheric component of the same i.e. Global Forecast System model Version 2 (GFSv2) forced with bias-corrected daily SST (GFSbc). They have shown that, though CFST126 is able to well capture the northward phase propagation, it shows dry bias in rainfall over the Indian landmass. Although reduced to some extent, the dry bias is present in the GFSbc also.

This report will document the developmental aspects of the EPS, its general real-time prediction performance during 2011, 2012 monsoon seasons and the skill statistics for 12 years, 2001-2012. Though a global EPS is developed, this evaluation is more focussed over the monsoon zone region or MZI [Rajeevan et al. 2010] and other four regions of the subcontinent where ISMR is more or less homogeneous [**Figure 1**]. To remove the stochasticity and quasi-periodicity of rainfall, the ERP skill of the EPS are evaluated at the pentad mean scale. The pentad prediction skill may be considered as the ISV prediction skill and is a more rigorous way of evaluating the model's hindcast skill. In addition to this, some aspects of large-scale MISOs, error growth statistics and the forecast of monsoon onset over Kerala (MOK) is also evaluated in this report. The impact of high resolution is studied by running the model at T382 (~38km) resolution and the results are compared with that of the T126 and GFSbc.

2. MODEL, OBSERVATIONAL DATA SETS

2.1. MODEL

The CGCM used for the development of ERP system is the latest version of National Centers for Environmental Prediction (NCEP) CFSv2 [Saha et al. 2013; submitted manuscript] which is run at T126 (~100km) and T382 (~38 km) horizontal resolutions with 64 vertical levels. The atmospheric component of the model is the NCEP GFSv2 at T126 resolution which is coupled to the GFDL Modular Ocean Model version 4p0d [MOM4; Griffies et al. 2004], sea-ice model and land surface model. MOM4 has zonal resolution of 1/2° and meridional resolution of 1/4° between 10°S and 10°N, gradually increasing through the tropics to 1/2° pole ward of 30°S and 30°N. There are 40 layers in the vertical with 27 layers in the upper 400 m of the ocean, and the maximum depth is approximately 4.5 km. The vertical resolution is 10 m from the surface to 240 m depth, gradually increasing to about 511 m in the bottom layer.

2.2. OBSERVATIONAL DATA SETS

To validate the model outputs, following available observational and reanalysis datasets have been used: a) daily gridded rainfall data from National Climate Centre, India Meteorological Department [Rajeevan et al. 2006] the TRMM-gauge merged rainfall dataset [Mitra et al. 2009] from India Meteorological Department (IMD) and d) daily NOAA OISST (*http://www.esrl.noaa.gov/psd/*).

3. ACTIVE/BREAK SPELLS SELECTION, MISO DEFINITION, MONITORING and MONSOON ONSET OVER KERALA

The MISO is a large-scale northward (from Indian Ocean towards Indian landmass) propagating 20-80 days oscillation and manifests as active/break cycles over MZI. MISO can be broadly defined by: 1) the traditional definition of active/break cycles and 2) the newly developed phase evolution and phase diagram method.

3.1. ACTIVE/BREAK SPELLS SELECTION

Over the time, scientists [Sikka and Gadgil 1980, Singh and Kriplani 1985, 1986, Magana and Webster 1996, Webster et al. 1998, Krishnan et al. 2000, Krishnamurthy and Shukla 2000, 2007, 2008, Annamalai and Slingo 2001, Goswami and Ajayamohan 2001, Waliser et al. 2003, Chattopadhyay et al. 2009, Joseph et al. 2009 etc.] have defined the active-beak spells of ISM in different ways based on rainfall, wind, pressure, OLR etc. Rajeevan et al. [2010] defined the active and break spells of ISMR during the peak monsoon months of July and August by using the normalized anomaly of the rainfall over MZI calculated from the high resolution daily gridded rainfall data over India. The break (active) spell has been identified when the normalized rainfall anomaly over the MZI which is roughly from 18.0°N to 28.0°N and 65.0°E to 88.0°E [Rajeevan et al. 2010], is less (greater) than –1.0 (+1.0), consecutively for three days or more. Though this criterion holds good for daily data, there is no well-defined criteria for pentad data. So in this study, we have defined active and break spells using long term pentad mean and standard deviation for the MZI region. We have plotted mean, ±1SD line as well as ±40% of the mean and found that ±40% line is within the ±1SD line. So we have suggested that when rainfall is less than -40% of the long term pentad mean, the spell has been defined as break; greater than 40%, the spell is active and otherwise normal. The active-break spells identified in this study using this criterion are comparable with those defined by Rajeevan et al. [2010]. The equivalence of pentad classification of active-break spells with that of Rajeevan et al. [2010] is also demonstrated in **Figure 2**. Here we have plotted the pentad mean anomaly and ±1SD departure from mean for the years 1993 and 1994, June to September (JJAS) monsoon season. For the other four homogenous regions where the proposed ±40% criterion is not holding well, we have used the world-wide accepted tercile category classification. Tercile are the three intervals *i.e.* the lower, middle, and upper thirds of the climatologically distributed values of a variable like rainfall where each category has an equal climatological probability of 33.33%. To help determine the three tercile ranges, the rainfall data has

been arranged in a descending order—i.e. we rank the data. The highest value is ranked 1, the second highest 2, and so forth. The three categories have been defined as *above normal*, *near normal or below normal* depending on whether the rainfall is in upper, middle or lower tercile respectively. For maintaining consistency, hereafter we will be referring the active and break spells as above normal and below normal respectively, for MZI region.

3.2 MISO DEFINITION AND MONITORING

The MISO index method has been proposed by Suhas et al. [2012] to monitor the temporal evolution and amplitude of ISO. They have defined the eight-phase evolution of ISO similar to that of Madden-Julian Oscillation, described in Wheeler and Hendon [2004]. The eight-phase evolution of ISO is shown in **Figure 3**. This is an EOF analysis performed on an extended data matrix. The extended data matrix is constructed by temporal embedding of a number of lagged copies of the data that are appended to the original data to create the extended matrix. The number of lags to be embedded depends on the dominant periodicity needed to be resolved and will filter out higher frequency variability. Since the dominant periodicity of the MISO in rainfall lies between 24 and 40 days, a lag of 15 days with 1day delay was found to be useful to resolve the smooth evolution of the MISO. The EOFs are constructed based on rainfall data averaged over the longitudinal band 60°-90°E spanning the latitudes 12°S-30°N for the 122 days of years 1998-2011. The EOF1 and EOF2 explain a combined variance of 23% and are separated from rest of the EOFs.

The northward propagation and real–time monitoring of MISO for the years 2007 and 2009 are shown in **Figure 4**. The systematic propagation of convective anomalies is obtained compositing precipitation for the days clustered in each octant or phase. In this figure, each octant or phase is represented as a pizza slice. Amplitude of MISO indices below the dotted unit circle ($MISO1^2 + MISO2^2 = 1$) is considered to be insignificant.

3.3 MONSOON ONSET OVER KERALA (MOK)

The beginning of monsoon season is marked by its onset over Kerala coast which is associated with lot of changes in the large-scale dynamical parameters as well as local moisture parameters. Prediction of monsoon onset over Kerala (MOK) is very much essential due to its socio-economical impact. Operationally, IMD has been declaring MOK subjectively based on the rainfall over various stations over Kerala, the value of outgoing long wave radiation (OLR) as well as the strength and vertical extent of the lower tropospheric zonal wind. Here, the emphasis is to devise a criterion from circulation and rainfall in the dynamical model for the prediction of MOK.

- For this, we define two indices – one from rainfall over Kerala (ROK) and another based on the strength of low level jet (LLJ). ROK is defined as the rainfall area-averaged over 74°-78°E and 8°-12°N; whereas LLJ is defined as the zonal wind at 850 hPa averaged over 55°-75°E and 5°-12°N.
- Onset is defined on day '*t*' if ROK > 5 mm/day and LLJ > 8m/s and if ROK and LLJ are either more than those at '*t-1*' for consecutive 5 days or when the average value of ROK and LLJ for these 5 days exceed 1.5 times their value at *t-1*.
- Conditions are relaxed in those cases when the MOK date is either obtained after 15 June or no MOK is obtained from the above mentioned criteria. The criteria is then checked for only three consecutive days and also the cut-off value for the average value of the indices for 5 days is made 1.2 times the original value, instead of 1.5 times. For this relaxed criteria, ROK > 2.5 mm/day and LLJ > 4 m/s at day *t*.
- The above-mentioned criterion is checked for each ensemble member and MOK is obtained for all of them. The mean day of all MOK is given as the MOK from the model.
- Since the long term mean date of MOK is around 1st June with a standard deviation of ~8 days [Ananthakrishnan and Soman, 1988], the forecasts starting from16th May initial condition have been utilized for defining the date of MOK.

4. VERIFICATION METHODS

To quantify the ERP skill of the present EPS various verification measures are used to calculate the skill scores for ensemble mean forecast (considered to be the deterministic forecast) and also the individual member forecast for probabilistic skill measures. Various skill scores calculated and presented in this study for ensemble mean deterministic forecast are: The Kuiper skill score (KSS) and bias score proposed by Hanssen and Kuiper [1965], the Heidke skill score (HSS) and Gerity score, the correlation coefficient and the root mean square error (RMSE). All these scores have been calculated for area-averaged rainfall over the above-mentioned regions.

In the present report, the probabilistic forecast verification is assessed by relative operating characteristic curves (ROC) that has gained widespread acceptance in recent time as a tool for probabilistic and ensemble forecast verification [Mason and Graham 1999, Hamill et al. 2000]. The ROC is drawn by using the Hit Rate (HR) and False Alarm Rate (FAR) by defining the dichotomous event as occurrence or non occurrence of the precipitation above or below certain thresholds for the area-averaged rainfall over MZI and four homogeneous regions for three observed categories discussed in section 3. The 11 member ensemble predictions of area-averaged percentage departure is sorted from the lowest to highest, which is then converted to yes/no forecast by comparing it with the observation and a binary value (1 for correct forecast and 0 for not forecasted) is assigned. Binary value 1 or 0 is assigned to the three observed categories also according to the percentage departure from precipitation. Separate 2x2 contingency tables are calculated for each sorted ensemble member with different probabilities. In this study, the forecast distribution from the EPS is arranged into 10% wide probability range bins, so that total 10 probability classes are obtained and HR and FAR are calculated for each probability interval. In this case, an event is said to be forecast if the forecast probability for that event is within the probability range (e.g., a forecast for above median rainfall that had 43% probability would fall in the 40-50% probability range). Observed occurrences (i.e., Hits) are then the number of times that a forecast probability fell into that bin and subsequently that event occurred (in the example, above median rainfall occurred).

Similarly, the observed non-occurrences (i.e., Misses) are the number of times a forecast was made for that probability bin but the forecast was 'incorrect' (in the example, below median rainfall occurred). The area under the ROC curve (AUC) is used to calculate the probabilistic skill score.

5. THE DEVELOPMENT OF ENSEMBLE PREDICTION SYSTEM

The EPS developed for ERP produces 11 member ensemble forecasts for 25 days lead time at every 5-day interval starting from 16th May to 28th September during 2001-2012. Details of the EPS are given below:

5.1. INITIAL CONDITIONS

The atmospheric and oceanic initial conditions are obtained from National Data Centres NOAA Operational Model Archive and Distribution System online model data server (*http://nomads.ncep.noaa.gov*). The initial conditions have been prepared from coupled data assimilation system (CDAS) with T574L64 GFS based atmospheric assimilation and MOM4 based oceanic assimilation.

5.2. PERTURBATION METHOD

Dynamical extended range prediction is subjected to various sources of errors, of which the errors arising from the uncertainties in the initial conditions and model are important. To eradicate such errors, ensemble prediction approach is one of the best options and has been attempted by various operational centers [Buizza and Palmer 1995, Toth and Kalnay 1993, Houtekamer et al. 1996, 2005]. Though there are several approaches to generate ensembles of different initial conditions, we use an approach [Abhilash et. al. 2013a] which is similar to the 'complex-and-same-model environment group' as classified in Buizza et al. [2008]. For the details on perturbation technique used in this study refer Abhilash et al., (2013a, b). Since the skill and spread of an EPS essentially depends on the ensemble size [Richardson 2001, Reynolds et al. 2011],

an ensemble of 10 perturbed atmospheric initial conditions has been developed in addition to one actual initial condition keeping in mind the huge computational power required to run large ensemble members on real-time basis. It has already been observed that there is not much difference between the perturbed and the actual analysis field over most of the parts except in the extra tropics where wind field is higher [Figure. 1, Abhilash et al. 2012].

5.3. THE EXPERIMENTAL SETUP

We have conducted three sets of experiments for the real-time prediction during 2011 and 2012 and the same three experiments were also conducted in the hindcast mode from 2001 to 2012.

The *first set* of experiment is with CFSv2 with its atmospheric component (GFSv2) at T126 horizontal resolution in coupled mode. Model integrations were started from 16 May and continued up to 28 September at every 5 day interval (16 May, 21 May, 26 May, ..., 23 Sep, 28 Sep). An ensemble of 11 members integration was performed for each start date and for the next 25 days period. This experiment is termed as CFST126.

In the *second set* of experiment we have identified the daily SST bias in the coupled model forecast in the control run of set one and corrected the bias with respect to the observed daily SST data (OISST). Bias correction is done by removing the daily mean bias (*i.e.* model daily climatology □ observed daily climatology) from the daily forecasted SST. This corrected daily SST is provided as the boundary forcing and GFSv2 at T126 horizontal resolution was run forced with this SST for the same period and same initial conditions in the ensemble mode as in set one. This experiment is termed as GFSbc.

In the *third set* of experiment CFSv2 has been integrated at T382 horizontal resolution with its atmospheric component (GFSv2) in coupled mode for the same period and same initial conditions in the ensemble mode as in set one. This experiment is termed as CFST382.

6. RESULTS AND DISCUSSION:

6.1 PERFORMANCE OF EPS FOR REAL-TIME PREDICTION DURING 2011 AND 2012

All the three sets of experiments were performed on real time basis during the year 2011 and 2012. However, the *first set* CFST126 run was completed for the hindcast period (2001-2012) at the time of issuing forecast and since the climatology was required to prepare forecast anomalies, the real time forecast was provided from this experiment only. Subsequently, other two sets of experiments were completed for hindcast period and we will present the forecast performance comparison from all the three sets during 2011 and 2012.

6.1.1 ONSET FORECAST

Figure 5a shows the time series of ROK and LLJ starting from 17th May 2011. It is evident from the figure that the forecasted date of MOK was 03rd June 2011. Our onset forecast suffered an error of 5 days, as the actual onset date declared by IMD was 29th May 2011. The forecast of MOK for year 2012 is shown in **Figure 5b**. The forecasted MOK (05th June) exactly matches with that of IMD.

6.1.2 FORECAST SKILL OVER HOMOGENEOUS REGIONS

To assess the forecast skill over the selected regions, correlation coefficients (CC) between the predicted and observed rainfall anomaly are listed in **Table 1** for the years 2011, 2012 over MZI for CFST126, GFSbc and CFST382. It is observed that CFST126 is performing better at pentad 4 lead (CC values are 0.43 and 0.38 respectively) in both the years.

The ERP skill of the tercile classifications over the homogeneous regions are shown in **Figure 6A-J.** Figure shows the categorical probabilistic prediction skills in pentad lead 3 and 4 for CFST126, GFSbc and CFST382**.**

6.1.3 MISO FORECASTING

Figure 7 and **8** show the evolution of MISO from four different initial conditions in 2011 and 2012 respectively. The start dates of forecast are randomly selected to capture active conditions starting around pentad 25–29th August, 2011 and 4-8th September, 2012. The forecast is shown for continuous 25 days. It is clear that, though CFST126, CFST382 and GFSbc show identical behaviour in capturing the phase evolution, the amplitude differs at times with observation. CFS-derived MISO amplitudes show larger over-estimation than GFSbc in general 5–7 days after the start date of forecast [Abhilash et al. 2013c].

6.1.4 FORECAST OF TRANSITION TO ABOVE NORMAL PHASE

Figure 9 and 10 shows the prediction verification for two above normal spells (25–29th August, 2011 and 4–8th September, 2012) in CFST126, CFST382 and GFSbc and in all the four pentad lead. These pentads represent a transition to the strong above normal conditions. **Figure 9** shows that CFST126 run is able to capture the transition to above normal spells over the west coast and northwest India four pentad in advance, while GFSbc shows mostly negative to no rainfall anomaly over this region 3–4 pentads in advance. Moreover, the performance of CFST382 in predicting this transition is comparable to that of CFST126. For 2012 (**Figure 10**), the 4–8th September above normal spell over south-central India and adjoining BoB is well-captured four pentads in advance in CFS126 run compared to GFSbc. Again, CFST382 run shows similar performance to that of CFST126. Thus, the transitions to above normal spells are predicted well in advance both in CFST126 and T382 run with better skill in terms of spatial patterns of observed distribution of rainfall [Sahai et al. 2013b].

6.2 Long term statistics

6.2.1. JJAS mean bias

Serial hindcast experiments have been performed for the years 2001-2012 using CFST126, CFST382 and GFSbc. The climatological bias in precipitation during the months JJAS in the pentad lead 1- 4 is shown in **Figure 11** for CFST126, GFSbc and CFST382. It is clear from the figure that CFST126 shows a dry bias over the Indian land mass which becomes prominent with the forecast lead and expands to the nearby oceanic regions. The dry bias over the Indian land region in GFSv2bc is slightly reduced in all the lead pentads compared to CFST126. The climatological precipitation biases are further improved in CFST382 run in all the four lead pentads [Sahai et al. 2013b].

6.2.2. MOK

For MOK, we have experimented only with CFST126 run. The forecasted MOK along with the actual IMD MOK for the hindcast period 2001-2010 is given in **Table 2**. The spread among different ensemble members for the forecasted MOK is also provided in the table.

6.2.3. FORECAST SKILL OVER HOMOGENEOUS REGIONS

The CCs between the observed and the forecasted rainfall anomaly at different pentad leads and for the five selected regions are shown in **Figure 12.** It is observed from the figure that except NEI, there is no significant improvement in the prediction skill of CFST382 run and both T382 and T126 skills are comparable in all the four pentad leads. On the other hand if we compare the same with that of GFSbc, it is observed that GFSbc shows better prediction skill in the pentad lead 2, 3 and 4 over CEI and MZI and in the pentad lead 3 and 4 over SPI.

The verification skill scores for the ensemble mean deterministic forecast are presented in **Figure 13A-E**. The different skill score measures used in this study are: The Kuiper

skill score (KSS) and bias score, the Heidke (HSS) and Gerrity skill score, the correlation coefficient and the root mean square error (RMSE). All these scores are shown over MZI and four homogeneous regions. Scores are calculated from CFST126, CFST382 and GFSbc. It is observed that over all the regions the large correlation at pentad lead 1 significantly drops at pentad lead 4. CC values of 0.5 are chosen as the threshold value for useful prediction on pentad scale. After pentad 2 lead, the deterministic ensembles mean prediction skill drops below 0.5 over all the selected regions both for CFST126 and CFST382. This confirms the uselessness of deterministic forecast alone after pentad 2 lead. The deterministic ensemble mean prediction skill from GFSbc is significant at pentad lead 3 over CEI, MZI and NWI. However, considering large sample size of 288, all CC values above 0.14 are significant at 99% confidence level. The HSS and GSS are found to be significant at 99% confidence level even at pentad lead 4 over CEI, MZI and NWI (from both CFST126, GFSbc). It is also evident from the figure that skill in predicting the below normal condition is higher, followed by above normal and then near normal over MZI at all lead pentads and from all CFST126, CFST382 and GFSbc. Similar results also can be seen over CEI from CFST126 and CFST382. Over SPI at pentad lead 1, 2 and 3, CFST126 and GFSbc present the similar result.

ROCs for the discussed three observed categories are also evaluated for the four homogenous regions and also for MZI using CFST382 and compared with CFST126 and GFSbc in **Figure 14A-E**. The area under the ROC curve is used for the calculation of the probabilistic skill score and is plotted in **Figure 15**. It is observed that below normal spells are more predicable in all the pentad leads over MZI, CEI and SPI and in pentad lead 1, 2 and 3 over NEI and in pentad lead 2, 3 and 4 over NWI. It is also observed that GFSbc outperforms CFS in predicting the above normal phases over MZI, CEI (pentad lead 2, 3, 4), SPI (pentad lead 2, 3, 4) and NWI (pentad lead 4).

6.2.4. MISO

The skill in predicting the large scale low-frequency mode of MISO is evaluated by computing the CCs between the predicted and observed MISO indices MISO1 and MISO2 and is

shown in **Figure 16**. The top panel shows the skill of all the initial conditions (ALL) as a function of lead-time. The middle and bottom panel plots are obtained by clustering the days in terms of the active initial conditions (ACT) and break initial conditions (BRK) respectively as mentioned in each panels. It is clear that increase in resolution has no significant impact in the prediction of large-scale MISO while GFSbc produces more skilful forecast of MISO for all initial conditions (ALL, ACT and BRK) [Sahai et al. 2013b].

7. CONCLUSIONS AND ROADMAP

An attempt is made to assess the skill of the dynamical ERP of ISMR by three sets of experiments with CFST126, GFSbc and CFST382. Real time predictions for the years 2011 and 2012 are studied in this document. Moreover the hindcast skill scores (deterministic as well as probabilistic) during the period 2001-2012 are also presented. The most important conclusions are tabulated below:

a. The increase in resolution in CFS model does not have any significant impact in improving the ERP skill of MISO on the real time.
b. It may be concluded that bias correction in SST has minimal impact on the prediction skill on short-to-medium range, whereas substantial influence is felt in the extended range between 12-18 days.
c. The onset forecast (MOK) for the selected years (2011 and 2012) are reasonable.
d. The statistical skill scores (HSS and GSS) are found to be significant at 99% confidence level even at pentad lead 4 over CEI and NWI.
e. The skill in predicting break is higher, followed by active and then normal over MZI and CEI at all lead pentads and at pentad lead 1 and 2 over SPI. Over NWI, skill in predicting break is higher at all lead pentads but active follows normal at pentad lead 4.

f. Analysis using ROC skill scores suggest that GFSbc outperforms CFS in predicting the active phases over MZI, CEI (pentad lead 2, 3, 4) and SPI (pentad lead 3, 4).

g. The forecast for the year 2011 and 2012 is apparently better in CFST382 as compared to CFST126. This is in contrast to the conclusion (a). The reason for this behaviour is not clear and requires further investigation.

For the year 2013 it is planned to generate ERP of MISOs using bias corrected GFS model *i.e.* GFSbc, but with more number (21) of ensemble members. However, to run GFS, SST forecast will be required from CFS. Therefore we will first perform 11 member ensemble run of CFS for 45 days on 33 nodes of PRITHVI (IBMP6 Cluster) which will take approximately 4 hours (one member run on 3 nodes simultaneously) and the 21 member SST bias corrected GFS for 25 days on 33 nodes which will take approximately an hour and 30 minutes. The onset forecast will be given by CFSv2 based on 16th May initial condition and subsequent forecast will be given from CFS and GFSbc after every five day till 28th September 2013.

ACKNOWLEDGEMENT

IITM is fully supported by the Ministry of Earth Sciences, Government of India, New Delhi, India. We are thankful to Prof. B. N. Goswami, Director, IITM for his encouragement. We are also thankful to Dr. A. Suryachandra Rao and Dr. R. H. Kripalani for their constructive comments and suggestions. Ms. Sharmila Sur is thankful to CSIR for financial support.

REFERRENCES

1. Abhilash, S., Joseph S., Chattopadhyay R., Pattnaik S., Krishna P. M., Dey S., Sahai A. K. and Goswami B. N., 2012, Performance of an Ensemble Prediction System based on CFSV2 for the Extended Range Prediction of Active-Break Spells of Indian Summer Monsoon Rainfall during 2011, IITM Research Report, No. RR-128.

2. Abhilash, S., Sahai A. K. , Pattnaik S., Goswami B. N., Kumar A., 2013a, Extended Range Prediction of Active-Break Spells of Indian Summer Monsoon Rainfall using an Ensemble Prediction System in NCEP Climate Forecast System. Int. J. Climatol., DOI: 511 10.1002/joc.3668.

3. Abhilash, S., Sahai A. K., Borah N., Chattopadhyay R., Joseph S., Sharmila S., De S. and Goswami B. N., 2013b, Prediction and Monitoring of Monsoon Intraseasonal Oscillations over Indian Monsoon Region in an Ensemble Prediction System using CFSv2, 2013, submitted to climate dynamics.

4. Abhilash, S., Sahai A. K., Borah N., Chattopadhyay R., Joseph S., Sharmila S., De S. and Goswami B. N., 2013c, Does bias correction in the forecasted SST improves the extended range prediction skill of active-break spells of Indian summer monsoon rainfall?, to be submitted.

5. Ananthakrishnan, R. and Soman M. K., 1988, The onset of the southwest monsoon over Kerala 1901-1980, J. of Clim., 8, 283-296.

6. Annamalai, H., and Slingo J. M., 2001, Active/break cycles: Diagnosis of the intraseasonal variability of the Asian summer monsoon, Climate Dyn., 18, 85–102, doi:10.1007/s003820100161.

7. Buizza R., Palmer T.N., 1995, The singular-vector structure of the atmospheric global circulation, Journal of Atmospheric Sciences, 52, 1434–1456.

8. Buizza, R., Leutbecher M. and Isaksen, L., 2008, Potential use of an ensemble of analyses in the ECMWF Ensemble Prediction System, Quarterly Journal of Royal Meteorological Society, 134, 2051–2066

9. Chattopadhyay, R., Goswami B. N., Sahai A. K., and Fraedrich K., 2009, Role of stratiform rainfall in modifying the northward propagation of monsoon intraseasonal oscillation, J. Geophys. Res., 114, D19114, doi:10.1029/2009JD011869.

10. Gadgil, S. and Gadgil S., 2006, The Indian Monsoon, GDP and Agriculture.Economic and Political Weekly, November 2006, 4887- 4895.

11. Goswami, B. N., and Mohan R. S. A., 2001, Intraseasonal Oscillations and Interannual Variability of the Indian Summer Monsoon, J. Climate, 14, 1180–1198, doi:10.1175/1520-0442(2001)014<1180:IOAIVO>2.0.CO;2.

12. Griffies, Stephen M., Matthew J. Harrison, Ronald C. Pacanowski and Anthony Rosati, 2004, A Technical Guide to MOM4, GFDL Ocean Group Technical Report No. 5, Princeton, NJ, NOAA/Geophysical Fluid Dynamics Laboratory, 342 pp.

13. Hamill, T. M. , Snyder C., Morss R. E., 2000, A comparison of probabilistic forecast from bred, singular-vector and perturbed observation ensembles. Mon. Wea. Rev, 128, 1835– 1851

14. Hanssen AW, Kuipers WJA, 1965, On the relationship between the frequency of rain and various meteorological parameters, Meded. Verh., 81, 2–15.

15. Houtekamer, P. L., Lefaivre L., Derome J., Ritchie H., Mitchell H.L., 1996, A system simulation approach to ensemble prediction. Monthly Weather Review, 124, 1225–1242.

16. Houtekamer, P. L., Mitchell H. L., Pellerin G., Buehner M., Charron M., Spacek L., Hansen B., 2005, Atmospheric Data Assimilation with an Ensemble Kalman Filter: Results with Real Observations Mon Wea Rev, 133, 604–620.

17. Joseph, S., Sahai A. K., and Goswami B. N., 2009, Eastward propagating MJO during boreal summer and Indian monsoon droughts, Clim. Dyn., 32 (7-8), 1139-1153. ISSN 0930-7575, doi:10.1007/s00382-008-0412-8

18. Krishnamurthy, V., and Shukla J., 2000, Intraseasonal and Interannual Variability of Rainfall over India, J. Climate, 13, 4366–4377, doi:10.1175/1520-0442(2000)013<0001:IAIVOR>2.0.CO;2.

19. Krishnamurthy, V., and Shukla J., 2007, Intraseasonal and Seasonally Persisting Patterns of Indian Monsoon Rainfall, J. Climate, 20, 3–20, doi:10.1175/JCLI3981.1.

20. Krishnamurthy, V., and Shukla J., 2008, Seasonal persistence and propagation of intraseasonal patterns over the Indian monsoon region, Climate Dyn., 30, 353–369, doi:10.1007/s00382-007-0300-7.

21. Krishnan, R., Zhang C., and Sugi M., 2000, Dynamics of Breaks in the Indian Summer Monsoon, J. Atmos. Sci., 57, 1354–1372, doi:10.1175/1520-0469(2000)057 <1354:DOBITI>2.0.CO;2.

22. Magana, V., and Webster P. J., 1996, Atmospheric circulations during active and break periods of the Asian monsoon, Preprints of the Eighth Conference on the Global Ocean-Atmosphere-Land System (GOALS), Amer. Meteor. Soc., Atlanta, GA.

23. Mason SJ, Graham NE, 1999, Conditional probabilities, relative operating characteristics, and relative operating levels. Wea Forecasting, 14, 713–725.

24. Mitra, A.K., Bohra A. K., Rajeevan M. and Krishnamurti T. N., 2009, Daily Indian precipitation analyses formed from a merged of rain-gauge with TRMM TMPA satellite derived rainfall estimates, Journal of Meteorological Society of Japan, 87A, 265-279.

25. Rajeevan, M., Bhate J., Kale J. D. and Lal B., 2006, High resolution daily gridded rainfall data for the Indian region: Analysis of break and active monsoon spells, Curr. Sc., 91, 296-306

26. Rajeevan, M., Gadgil S. and Bhate J., 2010, Active and break spells of the Indian summer monsoon. J Earth Syst Sci, 119, 229–247, doi:10.1007/s12040-010-0019-4.

27. Reynolds, C. A., Mclay J. G., Goerss J. S., Serra E. A., Hodyss D. and Sampson C. R., 2011, Impact of Resolution and Design on the U.S. Navy Global Ensemble Performance in the Tropics, Monthly Weather Review, 139, 2145-2155.

28. Richardson, D. S., 2001, Measures of skill and value of ensemble prediction systems, their interrelationship and the effect of ensemble size, Quarterly Journal of Royal Meteorological Society, 127, 2473-2489.

29. Saha, S. and co-authors, 2013, The NCEP Climate Forecast System Version 2. Submitted, Clim, http://cfs.ncep.noaa.gov/cfsv2.info/CFSv2_paper.pdf

30. Sahai, A. K., Sharmila S., Abhilash S., Chattopadhyay R., Borah N., Krishna R. P. M., Joseph S., Roxy M., De S., Pattnaik S. and Pillai P. A., 2013a, Simulation and extended range prediction of monsoon intraseasonal oscillations in NCEP CFS/GFS version 2 framework, Curr. Sci., Special Section (Atmosphere And Ocean Science), 104, 10.

31. Sahai, A. K., Abhilash S., Chattopadhyay R., Joseph S., Borah N., Goswami B. N., 2013b, How Important is the Model Resolution in the Operational Extended Range Forecast of Monsoon Precipitation over Indian Region in the NCEP CFSv2 model, to be submitted.

32. Sharmila, S., Pillai P. A., Joseph S., Roxy M., Krishna R. P. M., Chattopadhyay R., Abhilash S., Sahai A. K., Goswami B. N., 2013, Role of Ocean-Atmosphere Interaction on Northward Propagation of Indian Summer Monsoon Intra-Seasonal Oscillations (MISO). Climate Dynamics (Special issue on CFSv2), DOI: 10.1007/s00382-013-1854-1.

33. Sikka, D. R., Gadgil S., 1980, On the Maximum Cloud Zone and the ITCZ over Indian longitudes during the Southwest Monsoon, Mon Wea Rev, 108, 1840–1853

34. Suhas, E., Neena J.M. and Goswami B. N., 2012, An Indian monsoon intraseasonal oscillations (MISO) index for real time monitoring and forecast verification, Climate Dynamics, doi:10.1007/s00382-012-1462-5.

35. Toth, Z. and Kalnay E., 1993, Ensemble forecasting at NMC: The generation of perturbations, Bull. American Meteorological Society, 74, 2317–2330.

36. Waliser, D. E., and Coauthors, 2003, AGCM simulations of intraseasonal variability associated with the Asian summer monsoon, Climate Dyn., 21, 423–446, DOI:10.1007/s00382-003-0337-1.

37. Webster, P. J., Magaña V. O., Palmer T. N., Shukla J., Tomas R. A., Yanai M., and Yasunari T., 1998, Monsoons: Processes, predictability, and the prospects for prediction, J. Geophys. Res., 103, 14451–14,510, doi:10.1029/97JC02719.

38. Wheeler, M.C., Hendon H. H., 2004, An all-season real-time multivariate MJO Index: development of an index for monitoring and prediction, Monthly Weather Review, 132, 1917–1932.

39. Xavier, P.K. and Goswami B. N., 2007, An analog method for real time forecasting of summer monsoon subseasonal variability, Monthly Weather Review, 135, 4149-4160.

LIST OF FIGURES

Table 1: Correlation coefficients for the monsoon zone (MZI) rainfall for 24 pentads during year 2011 and 2012. The CC values are shown up to 4 pentad lead for GFST126, CFSbcT126 and CFST382.

	2011			2012		
	CFS T126	GFSbc T126	CFS T382	CFS T126	GFSbc T126	CFS T382
P1-Lead	0.64	0.63	0.70	0.74	0.90	0.76
P2-Lead	0.33	0.60	0.36	0.34	0.76	0.55
P3-Lead	0.12	0.41	0.38	0.53	0.30	0.56
P4-Lead	0.43	0.35	0.11	0.38	-0.22	0.25

Table 2: Forecasted and actual MOK for the years 2001-2010.

Year	**Actual MOK**	**Forecasted MOK**	**Spread among Ensemble Members**
2001	23 May	19 May	0
2002	29 May	27 May	7
2003	08 Jun	03 Jun	4
2004	18 May	19 May	0
2005	05 Jun	10 Jun	5
2006	26 May	24 May	3
2007	28 May	28 May	9
2008	31 May	31 May	10
2009	23 May	26 May	6
2010	31 May	31 May	4

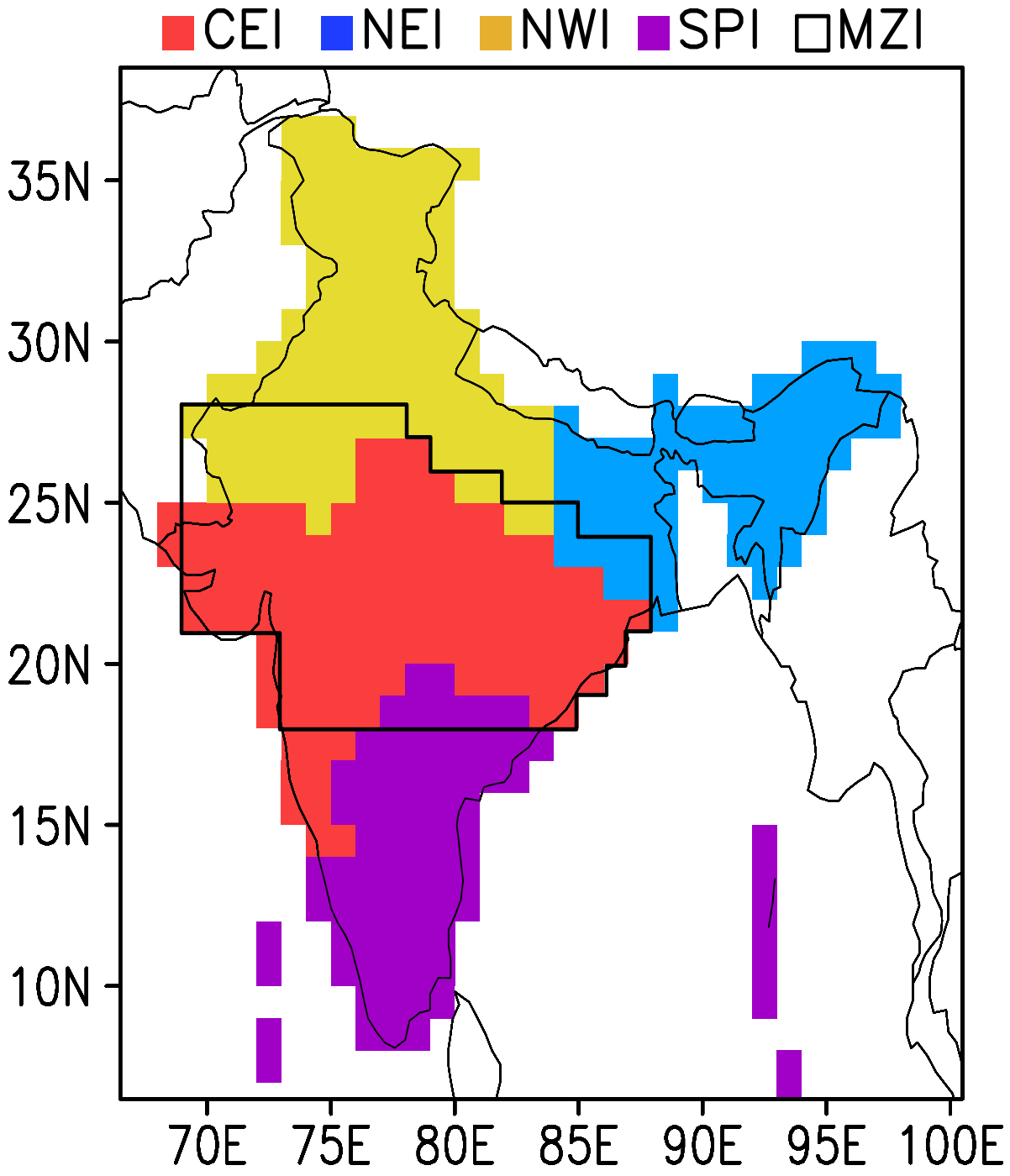

Figure 1: The Four homogenous regions and Monsoon Zone of India.

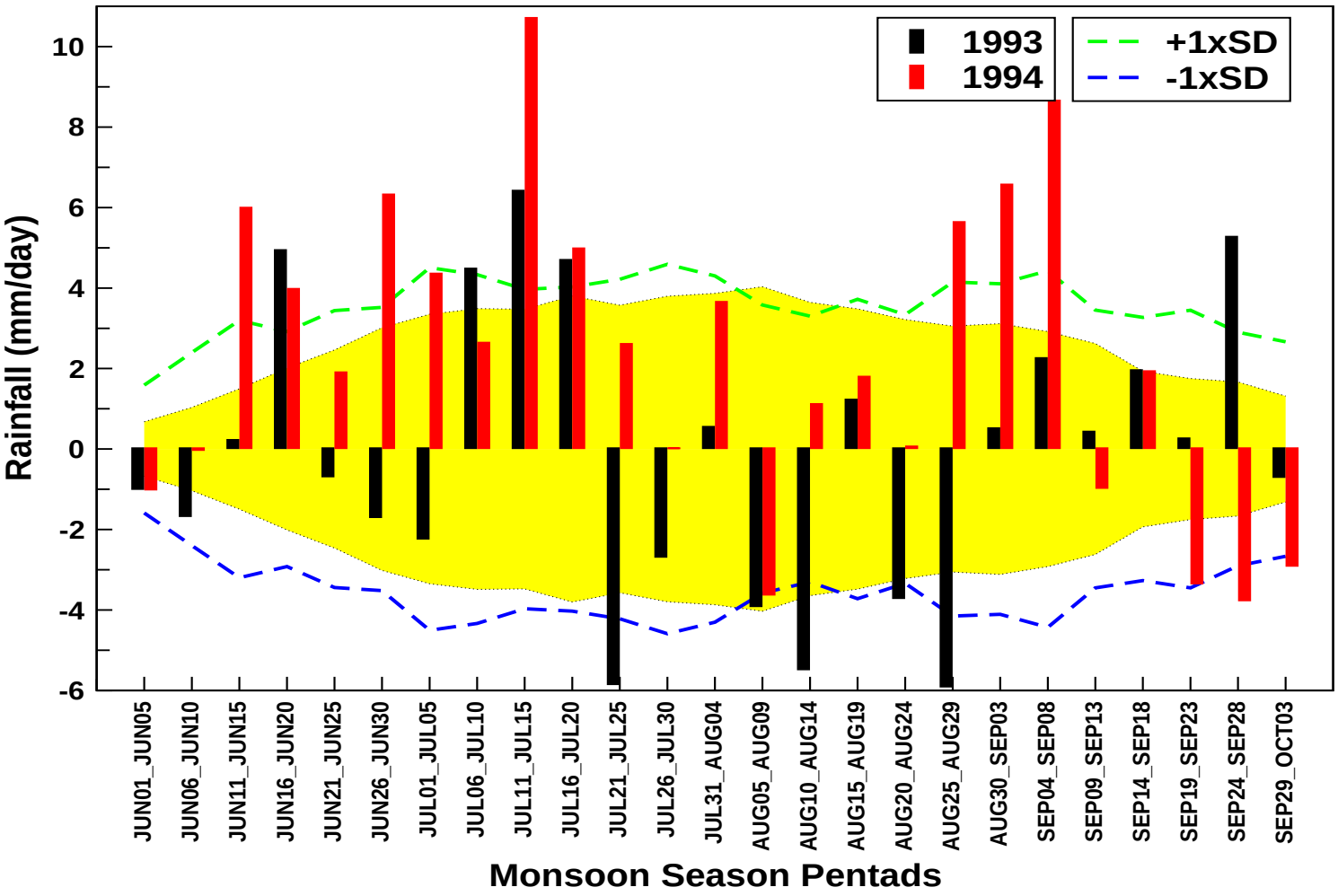

Figure 2: Pentad rainfall anomaly for the years 1993 (black bar) and 1994 (red bar) monsoon season. The yellow shaded region represents the normal rainfall amplitude defined using the $\pm$40% criteria. The green and blue dashed line represent the $\pm$1SD amplitude.

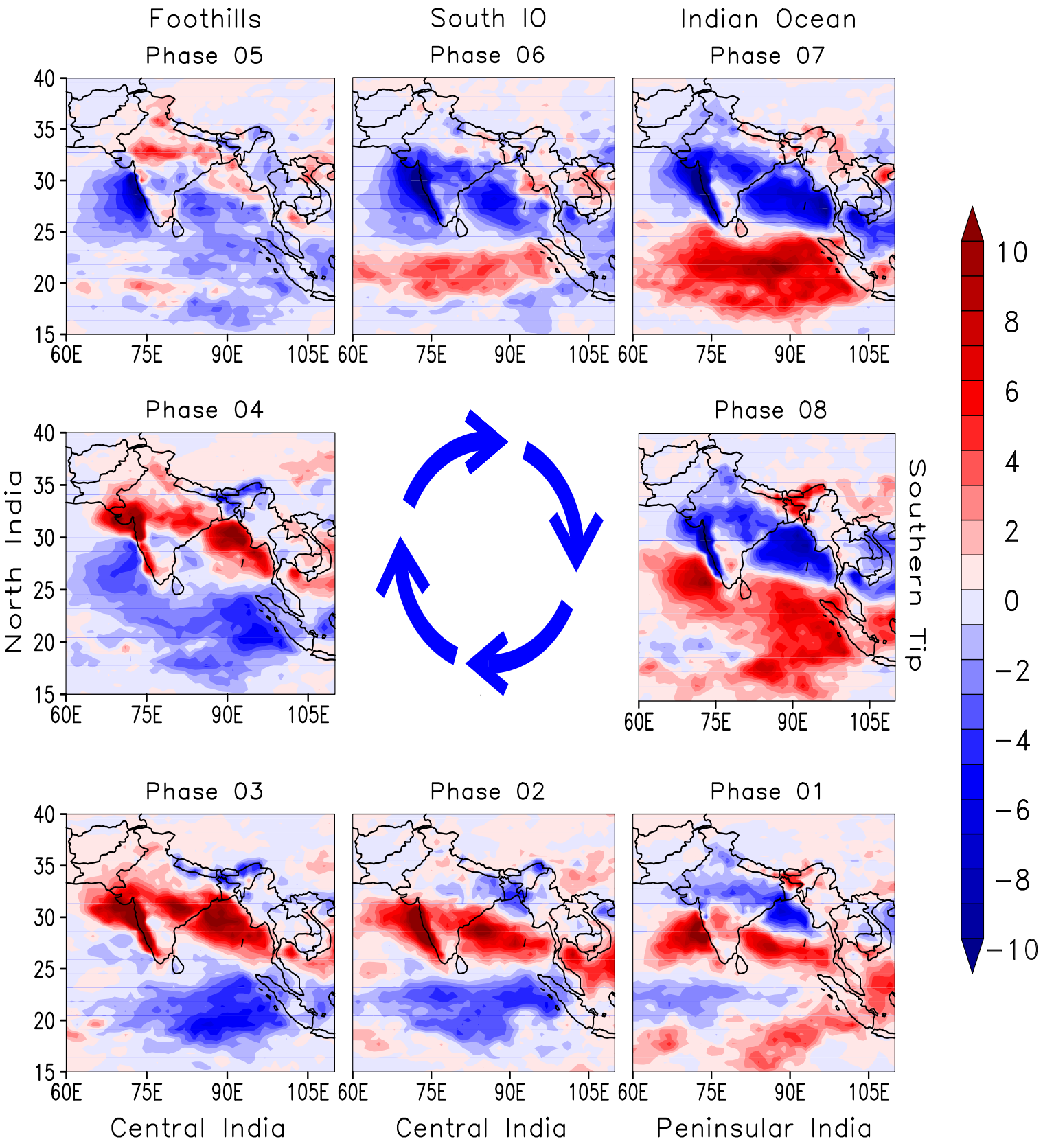

Figure 3: Composite plot for the days clustered in the 8 phases defined by MISO indices.

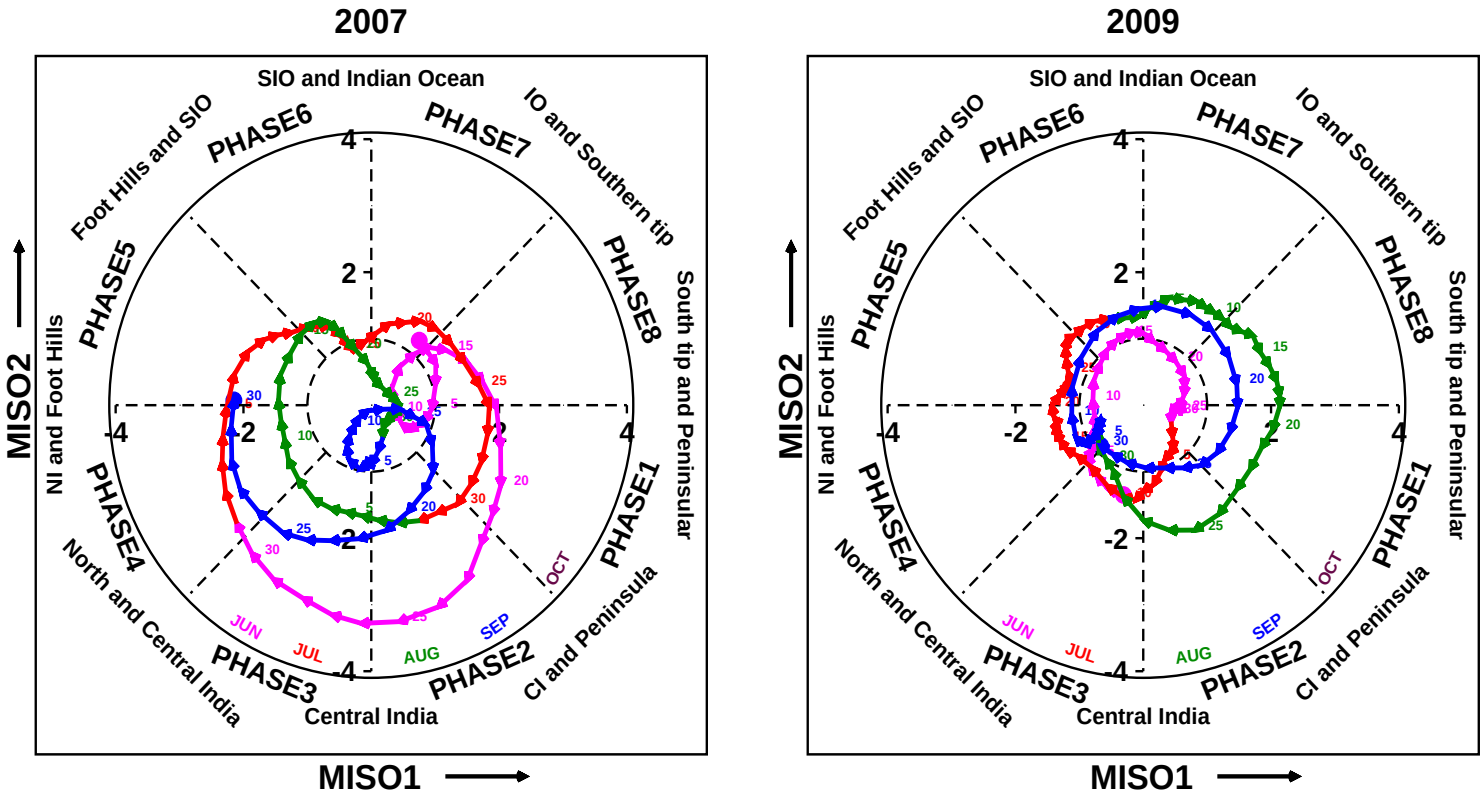

Figure 4: Phase diagram of MISO1 and MISO2 for two arbitrary years 2007 and 2009.

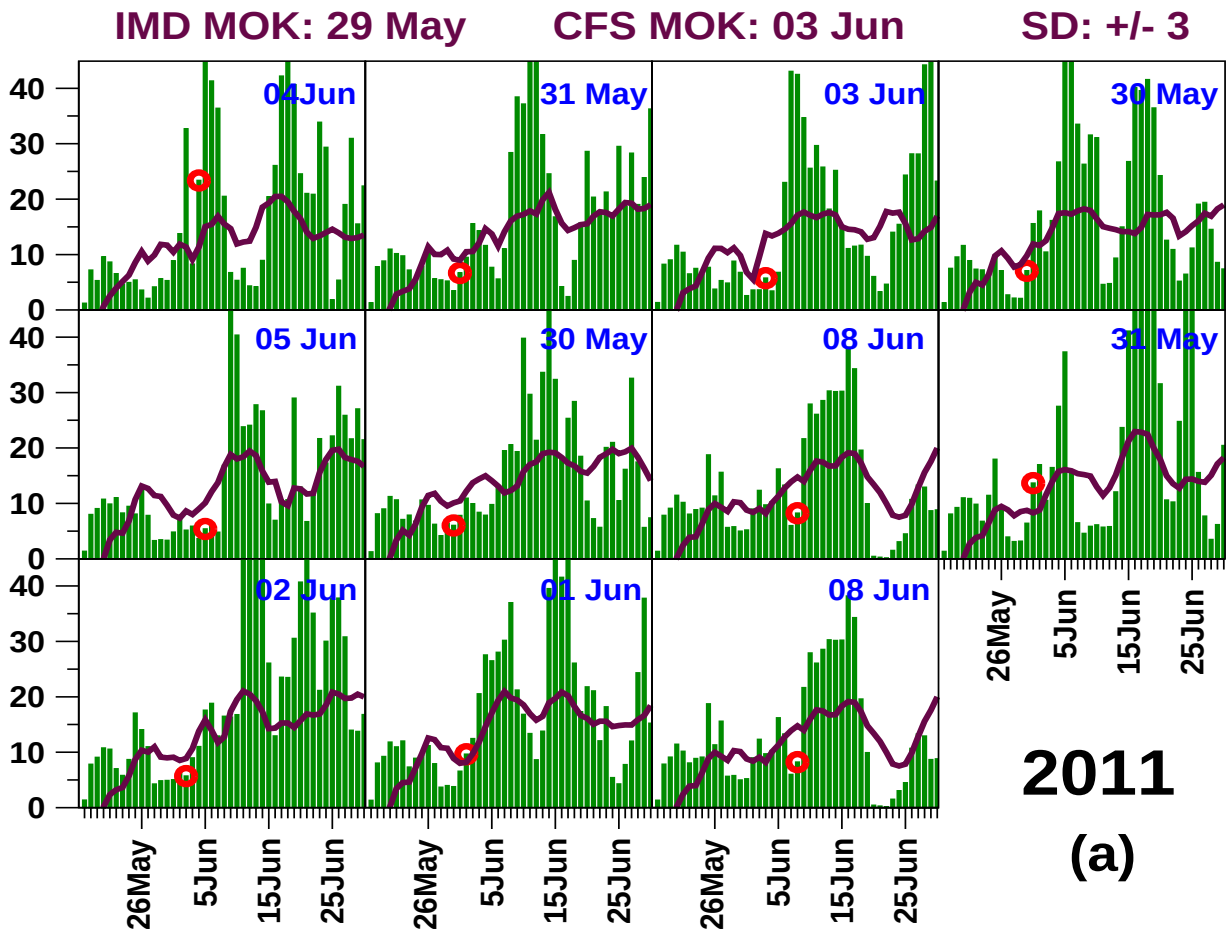

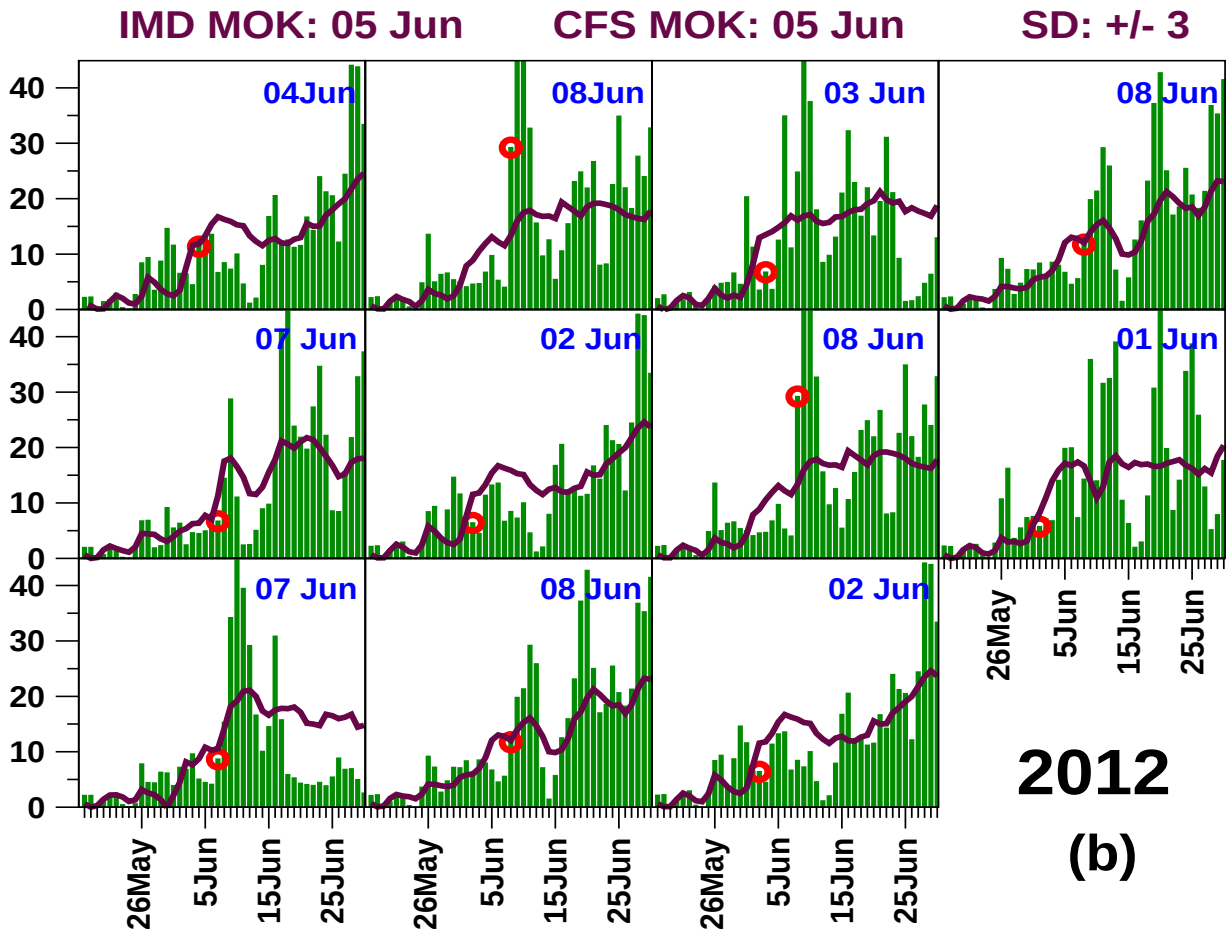

Figure 5: Monsoon onset forecast over Kerala for the year (a) 2011 and (b) 2012.

Figure 6: Observed and forecasted rain anomalies and forecast probabilities for three categories [Above normal (AN), Near normal (NN) and Below normal (BN)] over CEI during A. 2011, B. 2012; NEI during C. 2011, D. 2012; NWI during E. 2011, F. 2012; SPI during G. 2011, H. 2012 and MZI during I. 2011, J. 2012.

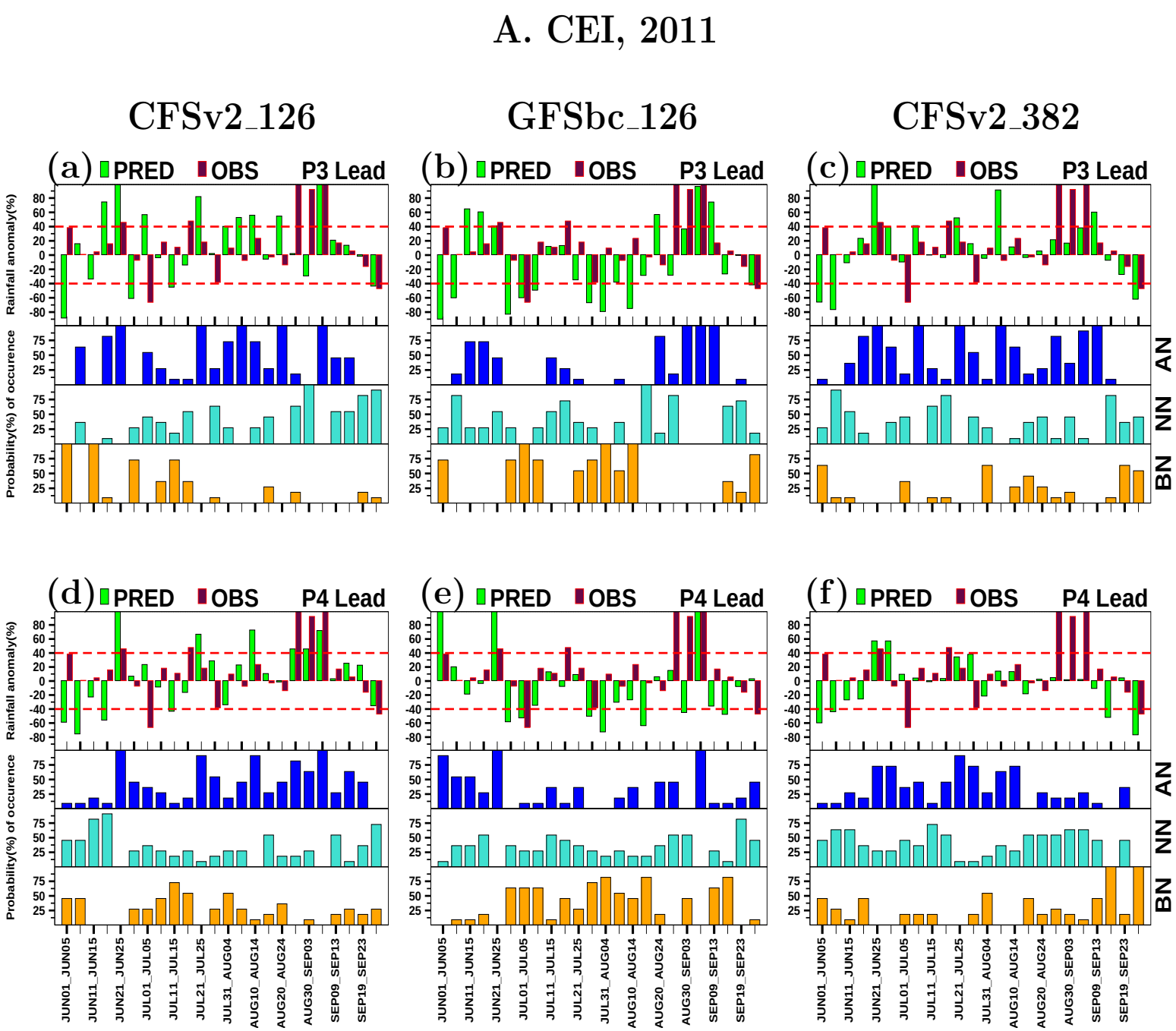

B. CEI, 2012

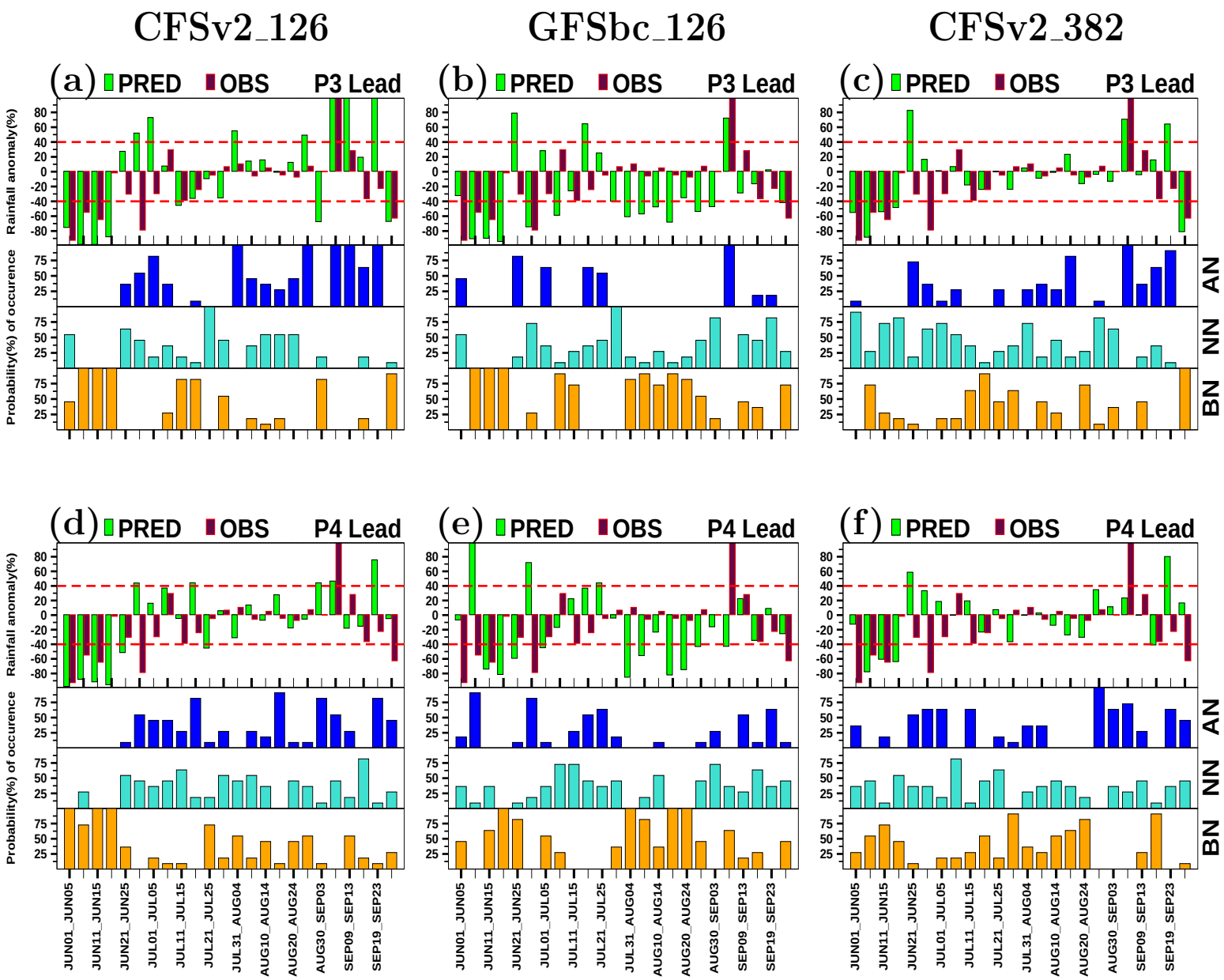
CFSv2_126
GFSbc_126
CFSv2_382
(a) PRED OBS P3 Lead
(b) PRED OBS P3 Lead
(c) PRED OBS P3 Lead
(d) PRED OBS P4 Lead
(e) PRED OBS P4 Lead
(f) PRED OBS P4 Lead
Rainfall anomaly(%)
Probability(%) of occurence
AN
NN
BN
JUN01_JUN05
JUN11_JUN15
JUN21_JUN25
JUL01_JUL05
JUL11_JUL15
JUL21_JUL25
JUL31_AUG04
AUG10_AUG14
AUG20_AUG24
AUG30_SEP03
SEP09_SEP13
SEP19_SEP23

C. NEI, 2011

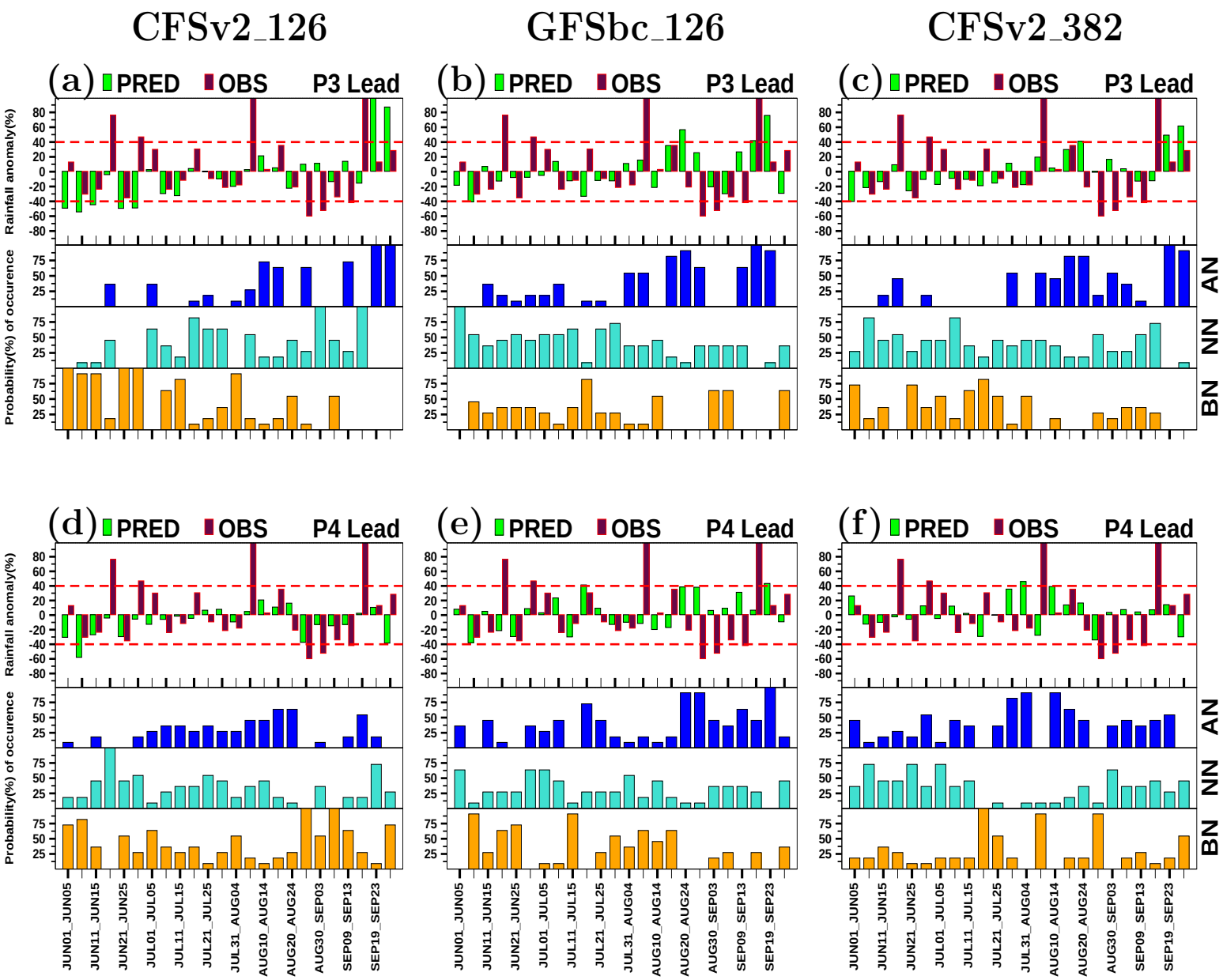
CFSv2_126
GFSbc_126
CFSv2_382
(a) PRED OBS P3 Lead
(b) PRED OBS P3 Lead
(c) PRED OBS P3 Lead
(d) PRED OBS P4 Lead
(e) PRED OBS P4 Lead
(f) PRED OBS P4 Lead
Rainfall anomaly(%)
Probability(%) of occurence
AN
NN
BN
JUN01_JUN05
JUN11_JUN15
JUN21_JUN25
JUL01_JUL05
JUL11_JUL15
JUL21_JUL25
JUL31_AUG04
AUG10_AUG14
AUG20_AUG24
AUG30_SEP03
SEP09_SEP13
SEP19_SEP23

D. NEI, 2012

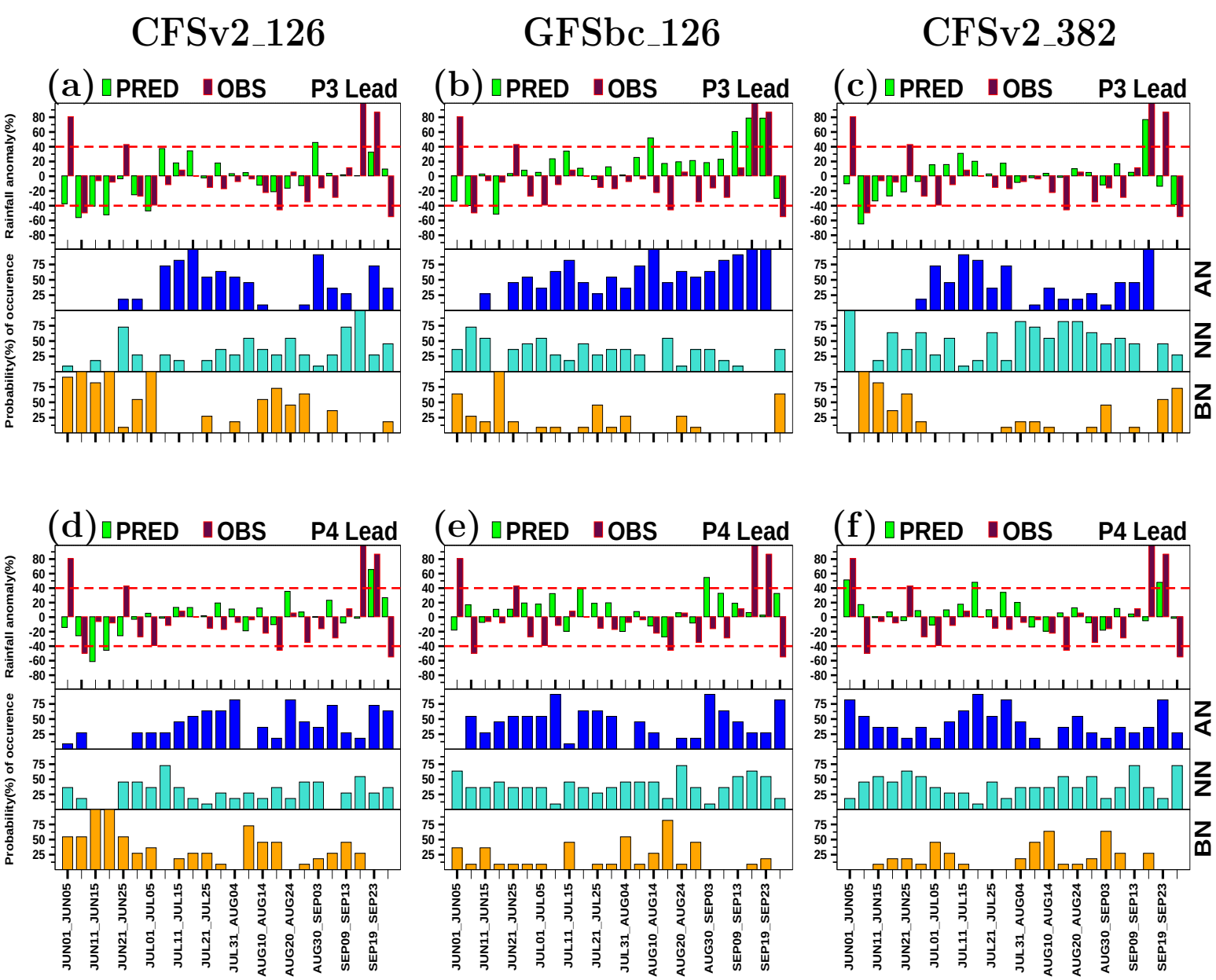
CFSv2_126
GFSbc_126
CFSv2_382
(a) PRED OBS P3 Lead
(b) PRED OBS P3 Lead
(c) PRED OBS P3 Lead
(d) PRED OBS P4 Lead
(e) PRED OBS P4 Lead
(f) PRED OBS P4 Lead
Rainfall anomaly(%)
Probability(%) of occurence
AN
NN
BN
JUN01_JUN05
JUN11_JUN15
JUN21_JUN25
JUL01_JUL05
JUL11_JUL15
JUL21_JUL25
JUL31_AUG04
AUG10_AUG14
AUG20_AUG24
AUG30_SEP03
SEP09_SEP13
SEP19_SEP23

E. NWI, 2011

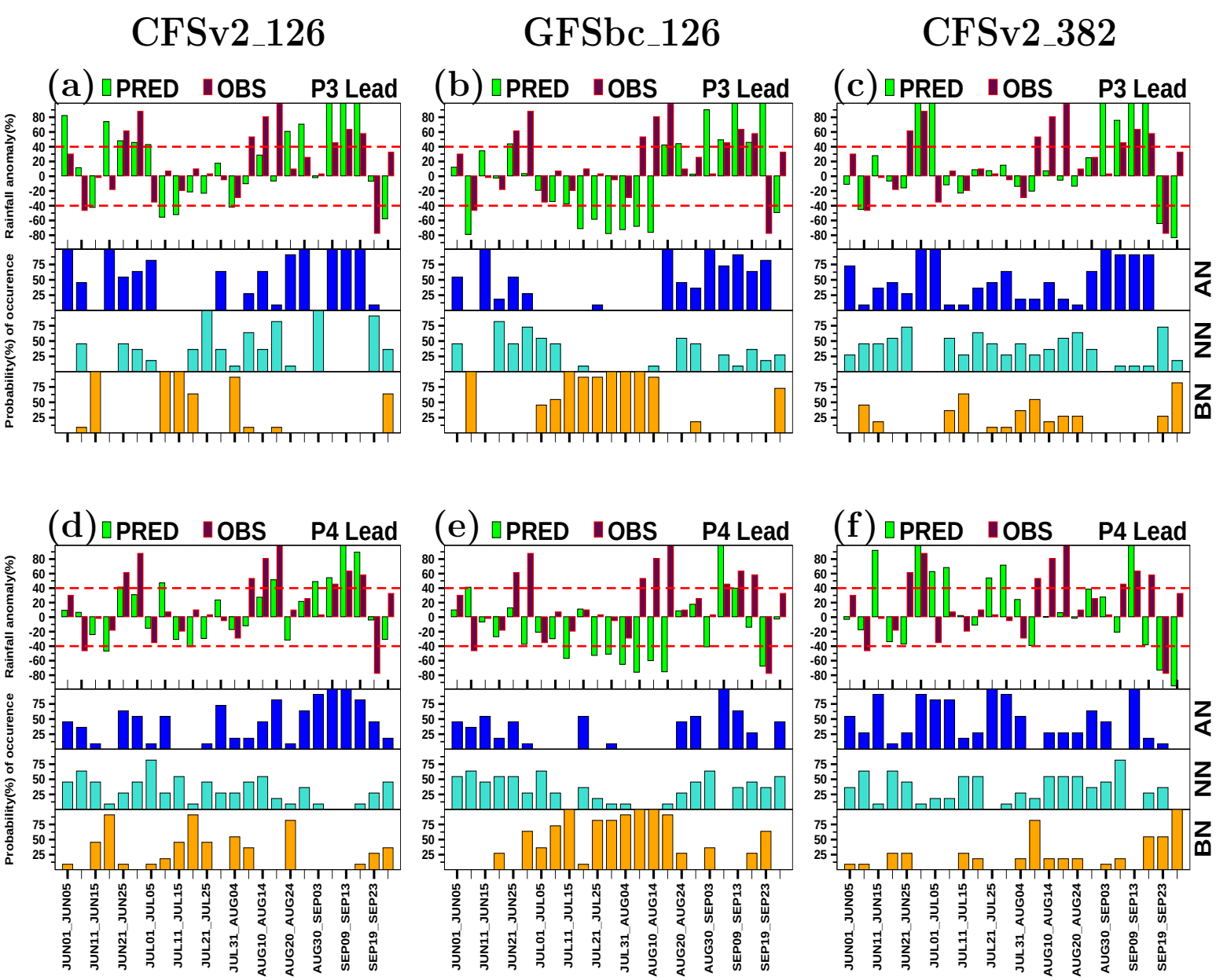
CFSv2_126
GFSbc_126
CFSv2_382
(a) PRED OBS P3 Lead
(b) PRED OBS P3 Lead
(c) PRED OBS P3 Lead
(d) PRED OBS P4 Lead
(e) PRED OBS P4 Lead
(f) PRED OBS P4 Lead
Rainfall anomaly(%)
Probability(%) of occurence
AN
NN
BN
JUN01_JUN05
JUN11_JUN15
JUN21_JUN25
JUL01_JUL05
JUL11_JUL15
JUL21_JUL25
JUL31_AUG04
AUG10_AUG14
AUG20_AUG24
AUG30_SEP03
SEP09_SEP13
SEP19_SEP23

F. NWI, 2012

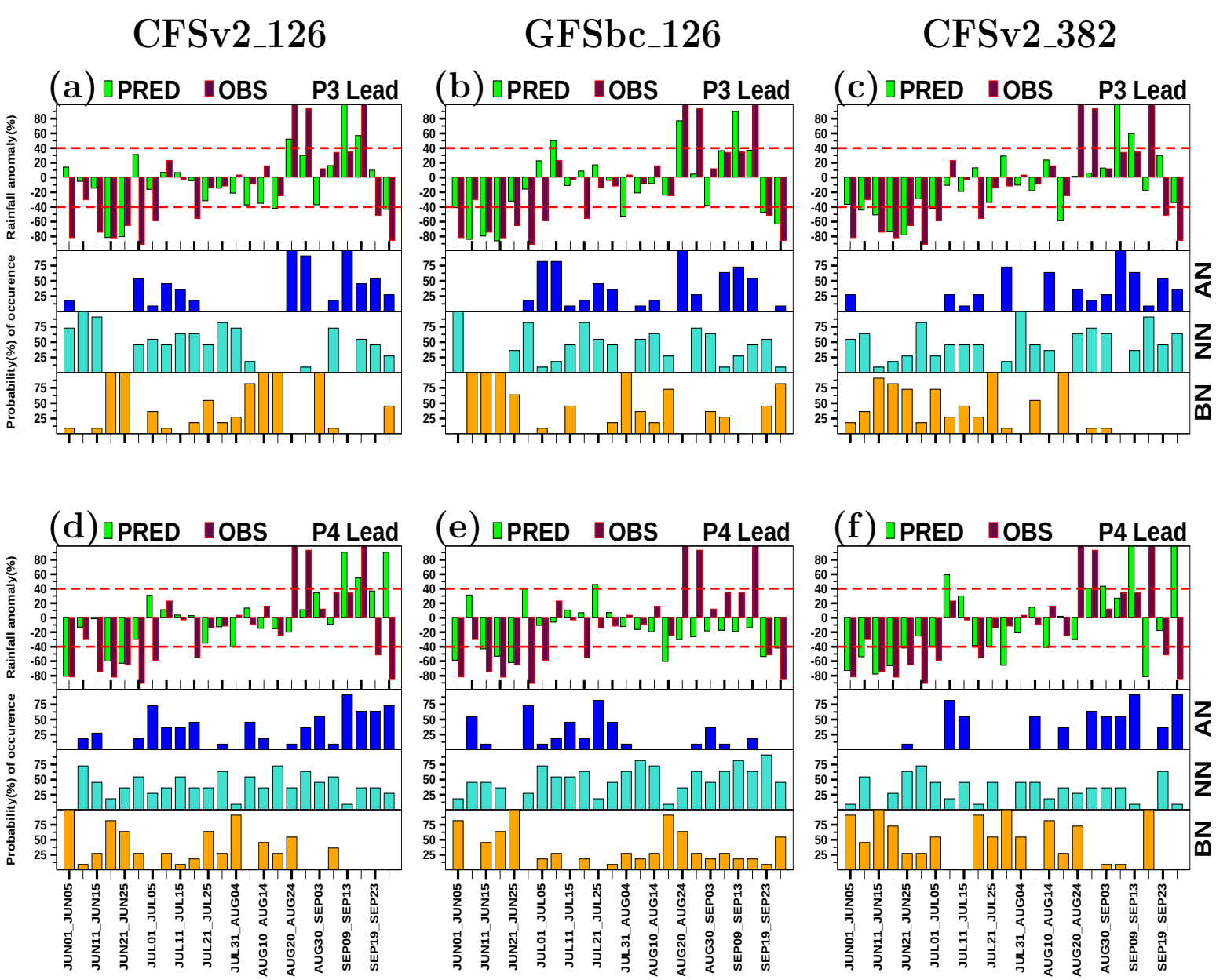
CFSv2_126
GFSbc_126
CFSv2_382
(a) PRED OBS P3 Lead
(b) PRED OBS P3 Lead
(c) PRED OBS P3 Lead
(d) PRED OBS P4 Lead
(e) PRED OBS P4 Lead
(f) PRED OBS P4 Lead
Rainfall anomaly(%)
Probability(%) of occurence
AN
NN
BN
JUN01_JUN05
JUN11_JUN15
JUN21_JUN25
JUL01_JUL05
JUL11_JUL15
JUL21_JUL25
JUL31_AUG04
AUG10_AUG14
AUG20_AUG24
AUG30_SEP03
SEP09_SEP13
SEP19_SEP23

G. SPI, 2011

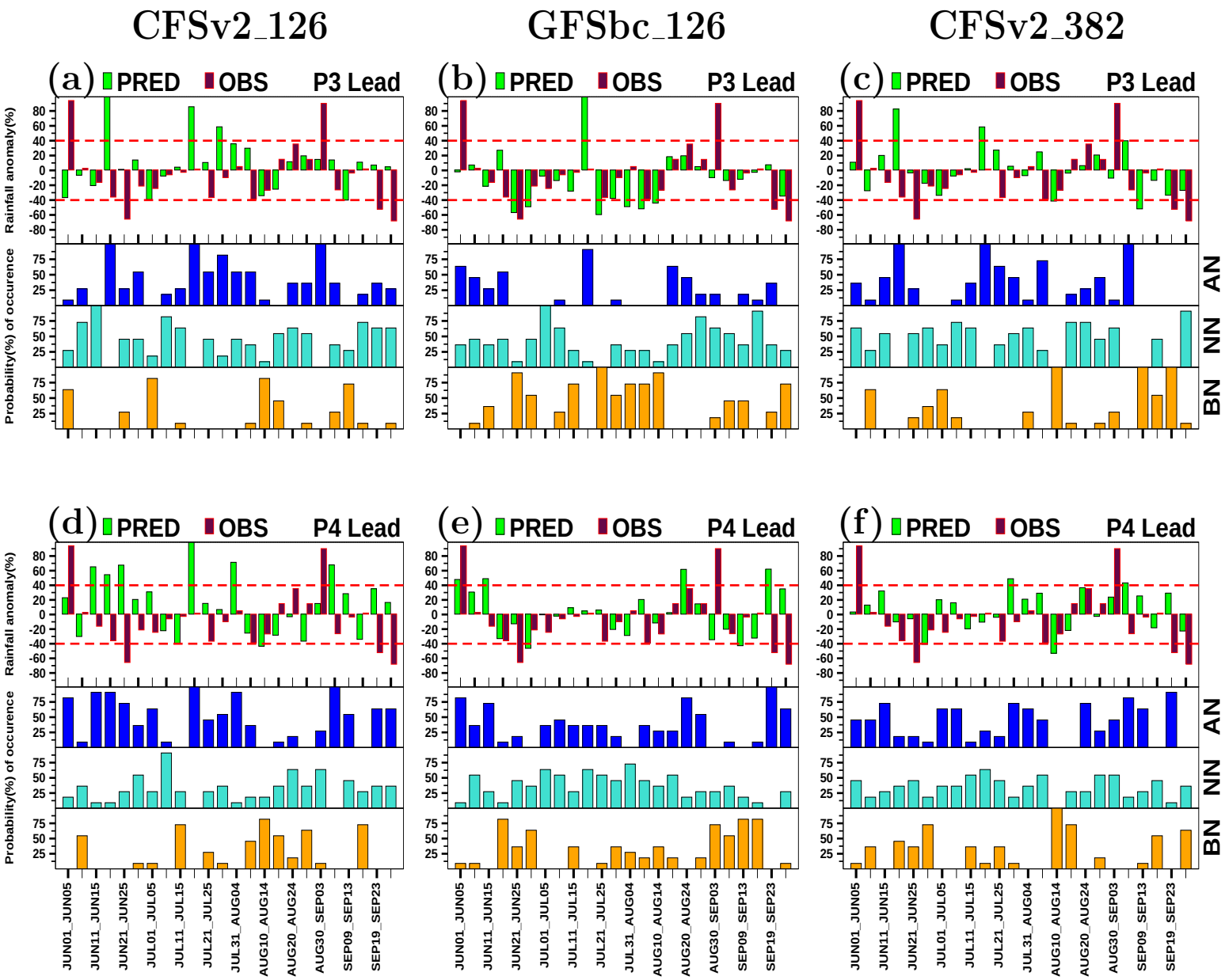
CFSv2_126
GFSbc_126
CFSv2_382
(a) PRED OBS P3 Lead
(b) PRED OBS P3 Lead
(c) PRED OBS P3 Lead
(d) PRED OBS P4 Lead
(e) PRED OBS P4 Lead
(f) PRED OBS P4 Lead
Rainfall anomaly(%)
Probability(%) of occurence
AN
NN
BN
JUN01_JUN05
JUN11_JUN15
JUN21_JUN25
JUL01_JUL05
JUL11_JUL15
JUL21_JUL25
JUL31_AUG04
AUG10_AUG14
AUG20_AUG24
AUG30_SEP03
SEP09_SEP13
SEP19_SEP23

H. SPI, 2012

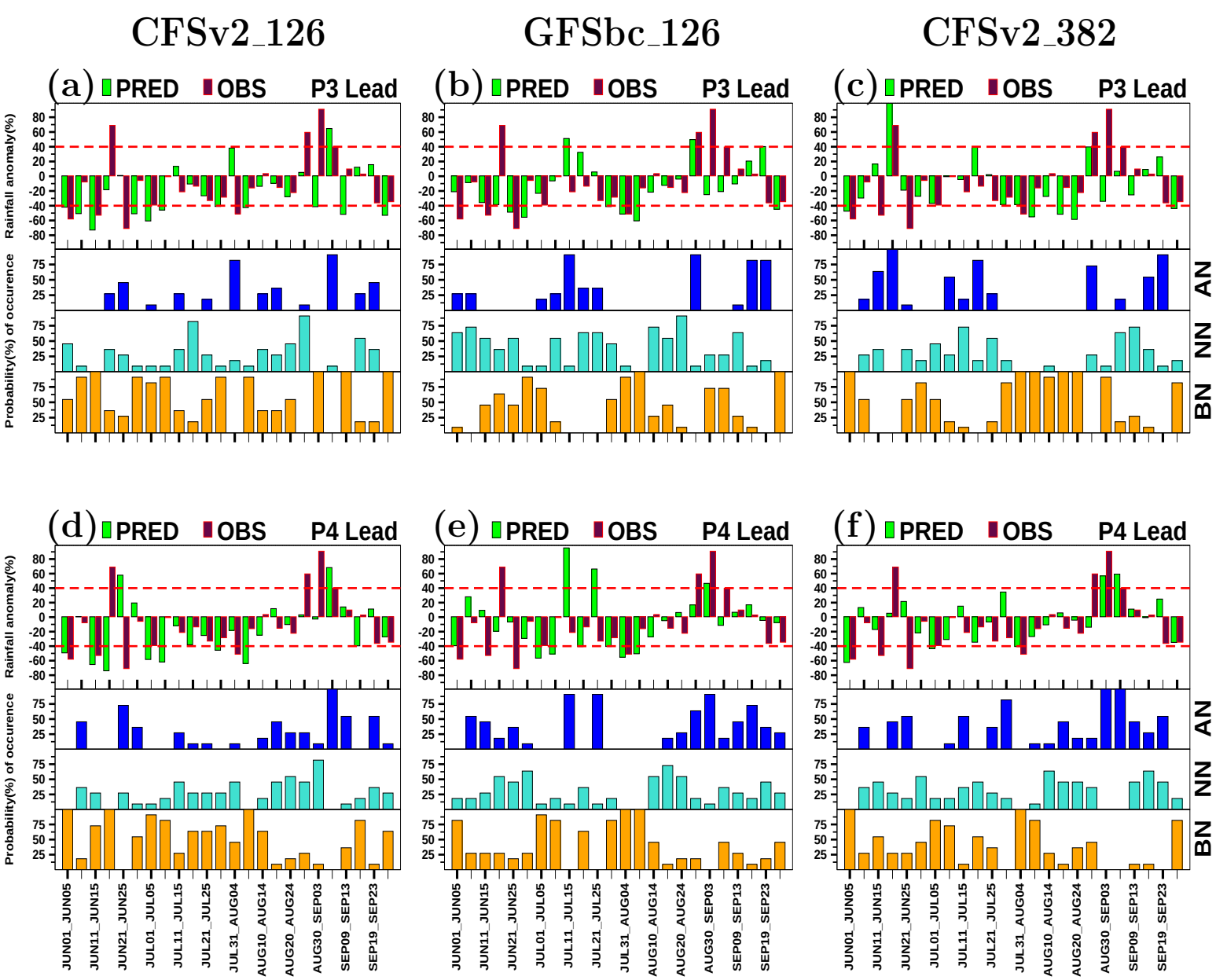
CFSv2_126
GFSbc_126
CFSv2_382
(a) PRED OBS P3 Lead
(b) PRED OBS P3 Lead
(c) PRED OBS P3 Lead
(d) PRED OBS P4 Lead
(e) PRED OBS P4 Lead
(f) PRED OBS P4 Lead
Rainfall anomaly(%)
Probability(%) of occurence
AN
NN
BN
JUN01_JUN05
JUN11_JUN15
JUN21_JUN25
JUL01_JUL05
JUL11_JUL15
JUL21_JUL25
JUL31_AUG04
AUG10_AUG14
AUG20_AUG24
AUG30_SEP03
SEP09_SEP13
SEP19_SEP23

I. MZI, 2011

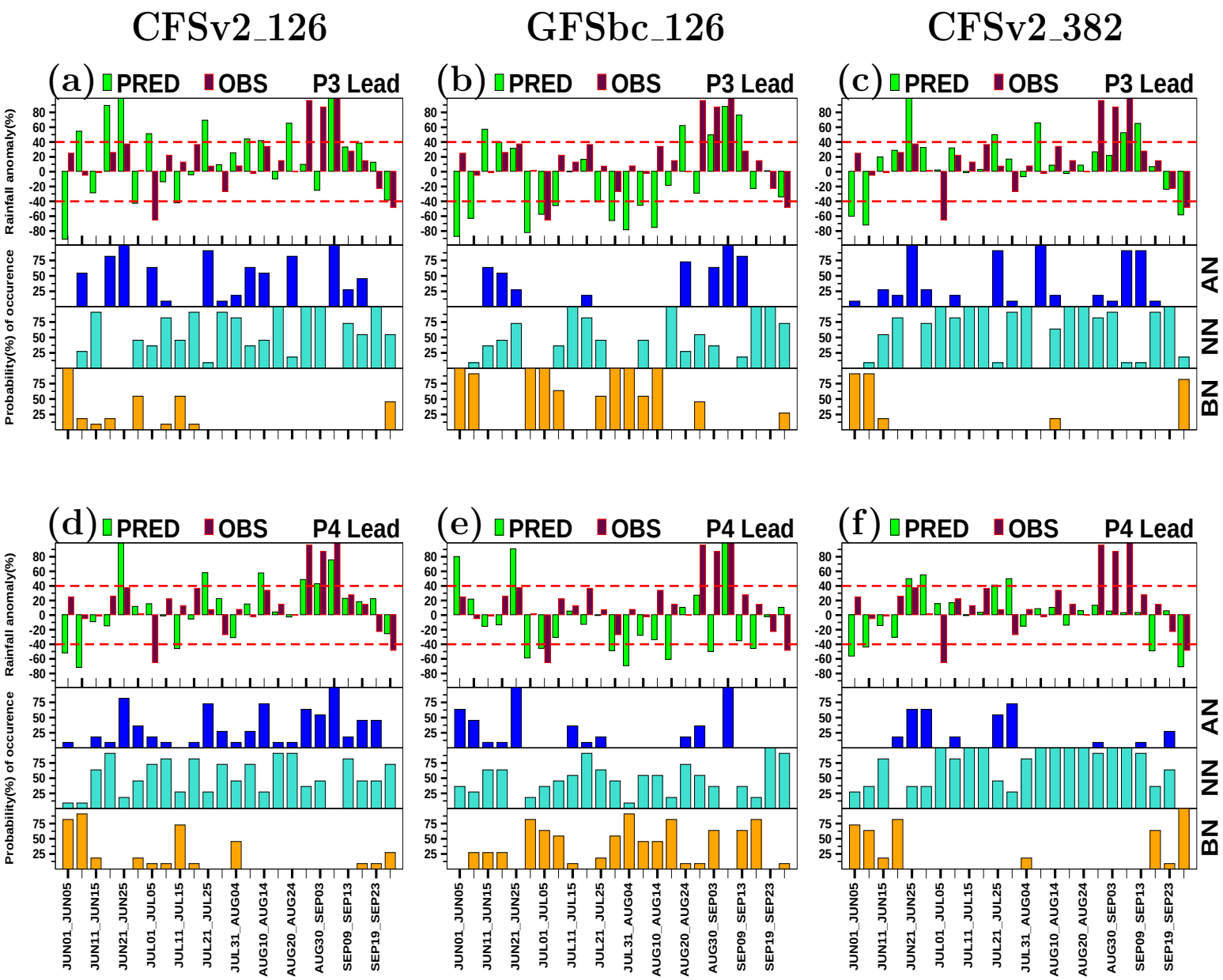
CFSv2_126
GFSbc_126
CFSv2_382
(a) PRED OBS P3 Lead
(b) PRED OBS P3 Lead
(c) PRED OBS P3 Lead
(d) PRED OBS P4 Lead
(e) PRED OBS P4 Lead
(f) PRED OBS P4 Lead
Rainfall anomaly(%)
Probability(%) of occurence
AN
NN
BN
JUN01_JUN05
JUN11_JUN15
JUN21_JUN25
JUL01_JUL05
JUL11_JUL15
JUL21_JUL25
JUL31_AUG04
AUG10_AUG14
AUG20_AUG24
AUG30_SEP03
SEP09_SEP13
SEP19_SEP23

CFSv2_126 GFSbc_126 CFSv2_382

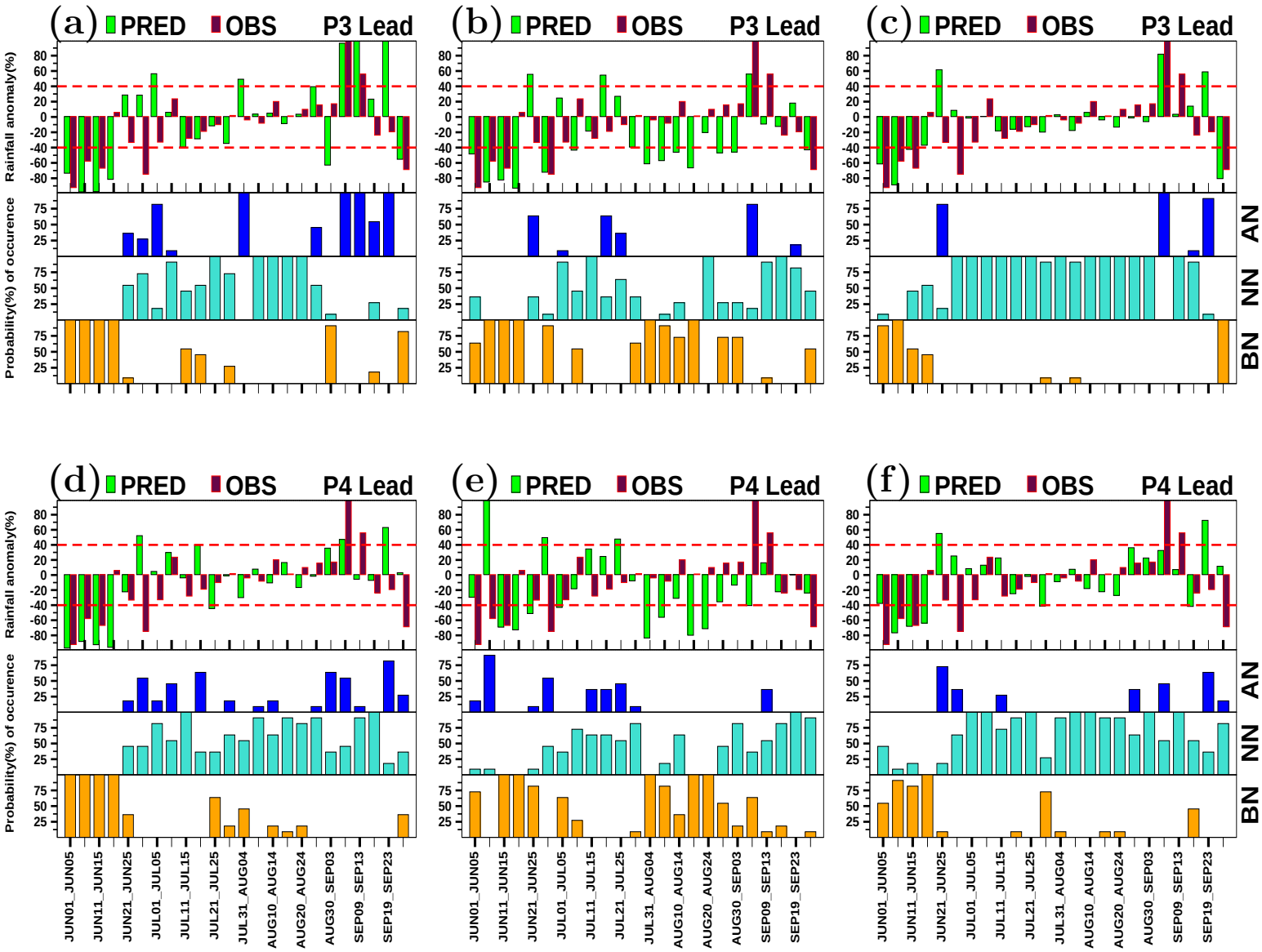

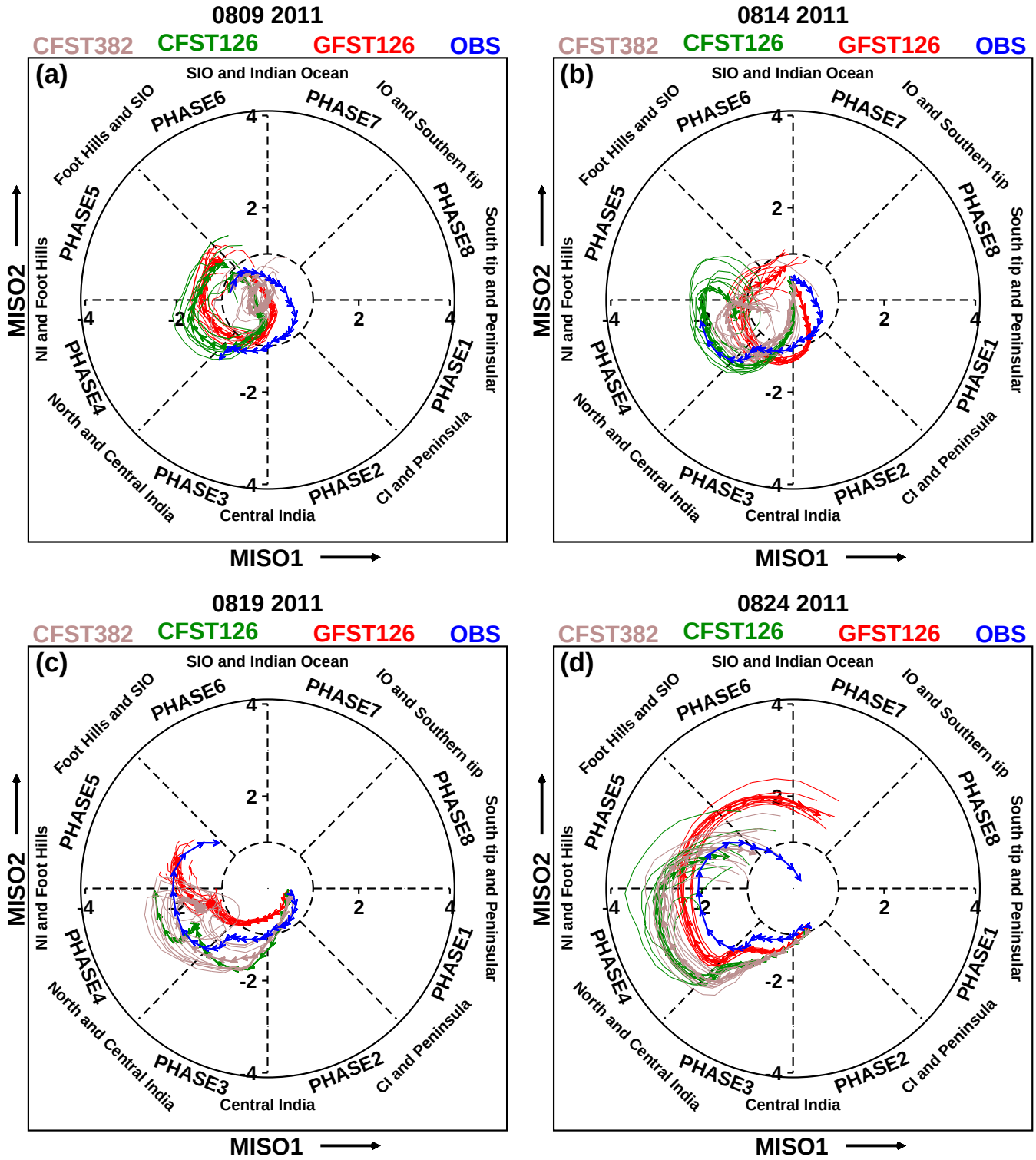

Figure 7: Phase evolution of an active episode during 25-29 August, 2011 for next 25 days from four initial conditions (c) 9 Aug (d) 14 Aug (e) 19 Aug and (f) 24 Aug. Blue line is for OBS, Red is for GFSbc forecast, Green is for CFST126 forecast and Grey is for CFST382 forecast.

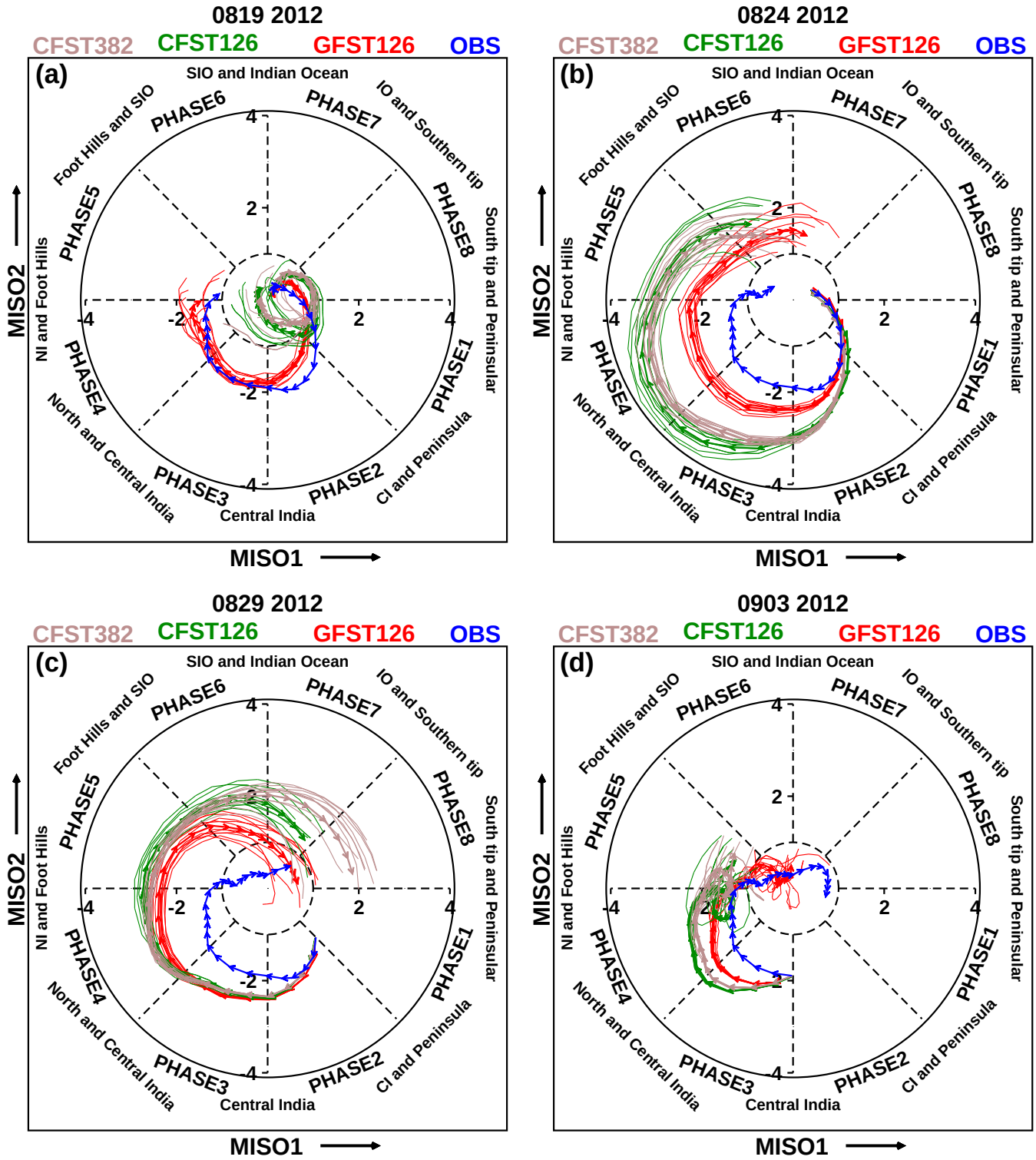

Figure 8: Phase evolution of an active episode during 4-7 Sep, 2012 for next 25 days from four initial conditions (c) 19 Aug (d) 24 Aug (e) 29 Aug and (f) 3 Sep. Blue line is for OBS, Red is for GFSbc forecast, Green is for CFST126 forecast and Grey is for CFST382 forecast.

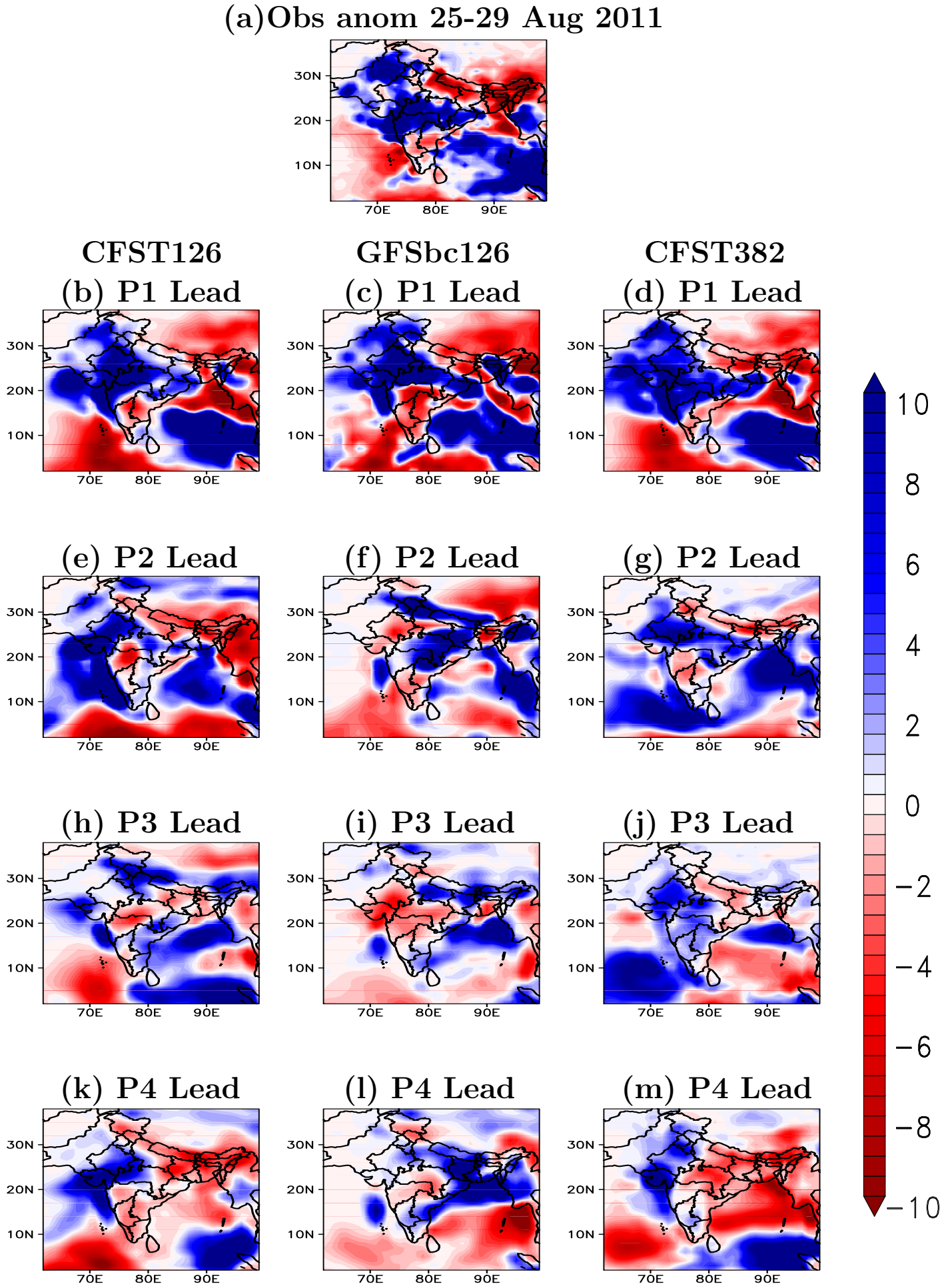

Figure 9: Prediction of transition to above normal phase around 25th August in 2011. (a) Observed anomaly; (b), (e), (h) and (k) CFST126 forecast; (c), (f), (i) and (l) GFSbc forecast and (d), (g), (j), (m) CFST382 forecast at P1, P2, P3 and P4 lead.

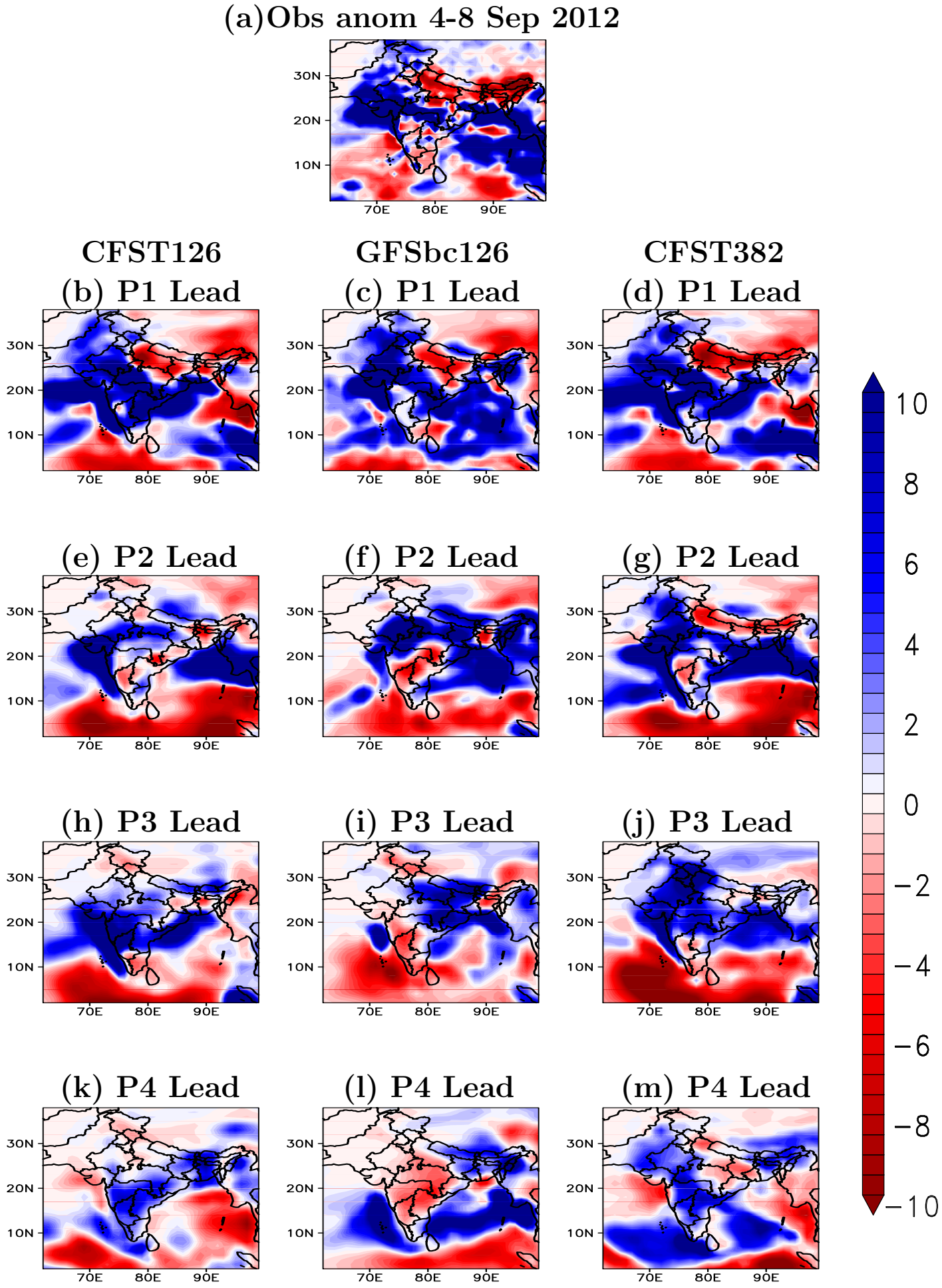

Figure 10: Prediction of transition to above normal phase around 4th September in 2012. (a) Observed anomaly; (b), (e), (h) and (k) CFST126 forecast; (c), (f), (i) and (l) GFSbc forecast and (d), (g), (j), (m) CFST382 forecast at P1, P2, P3 and P4 lead.

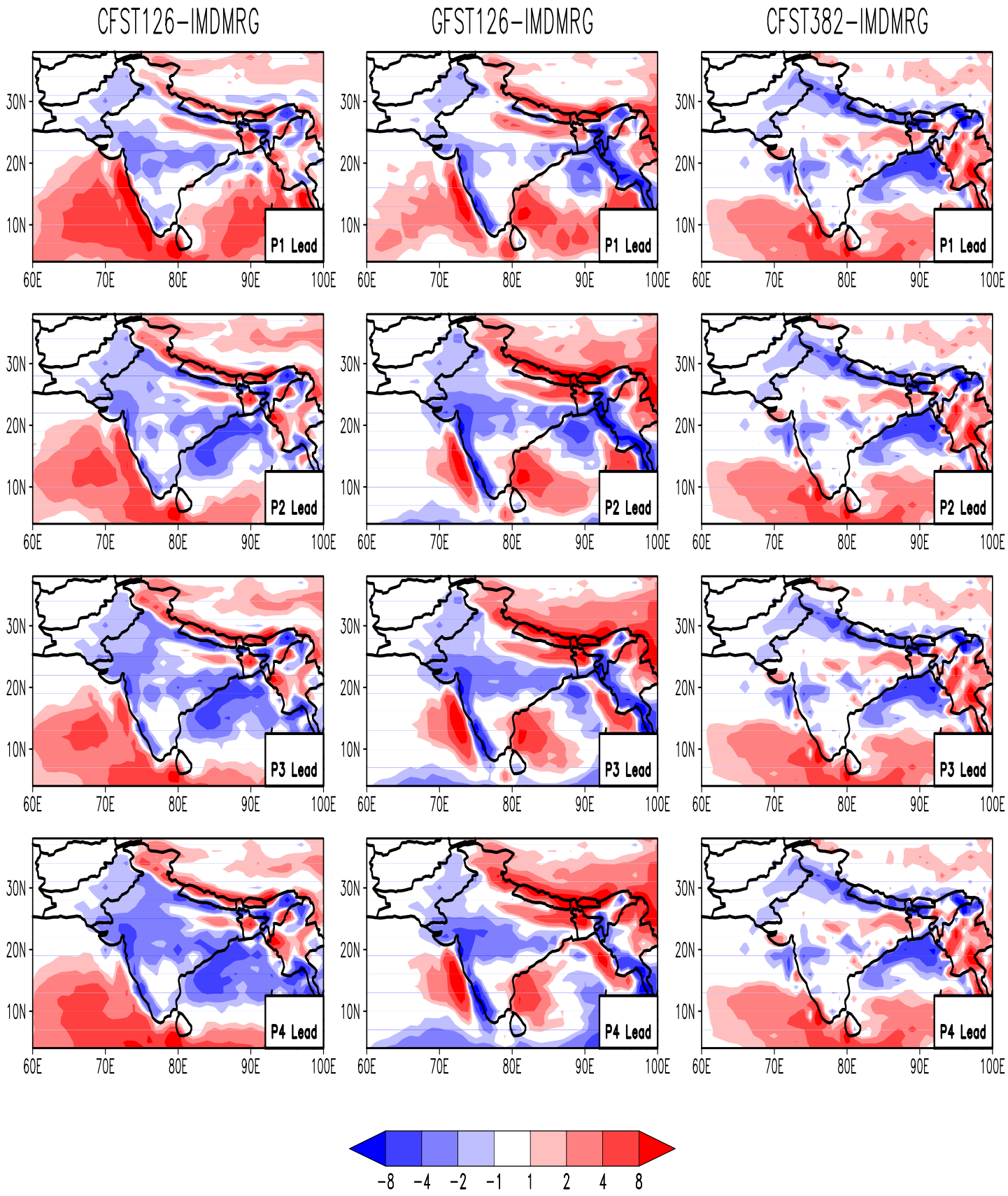

Figure 11: Climatological bias in precipitation during JJAS season in mm/day for CFST126 (left panel), GFSbc (middle panel) and CFST382 (right panel).

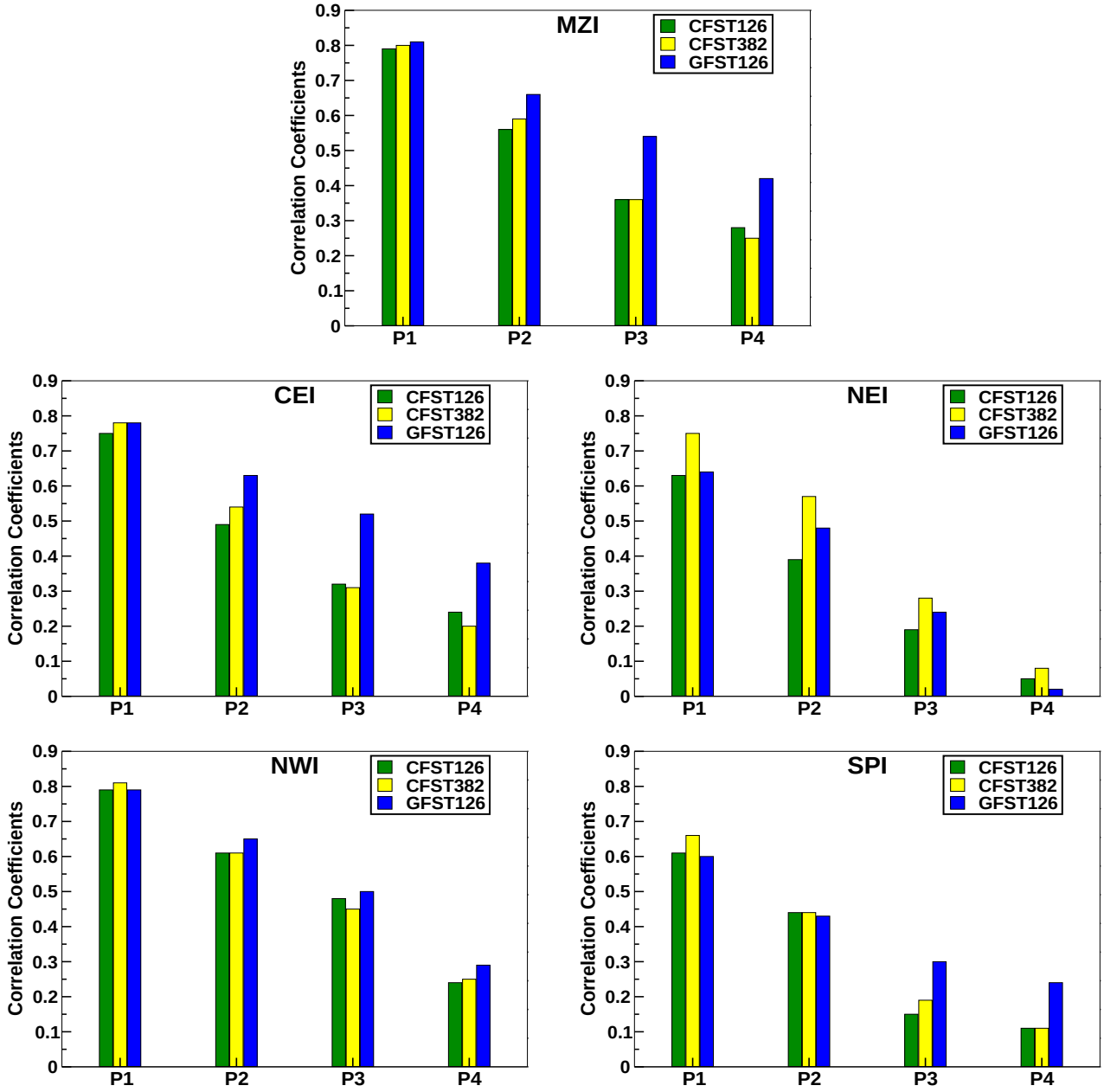

Figure 12: Correlation coefficients between the observed and forecasted rainfall anomaly for CFST126, CFST382 and GFSbc over the four homogeneous regions and MZI.

Figure 13: Pentad lead skill scores (a) Correlation Coefficients and RMSE, (b) HSS and Gerrity skil score, (c) Bias scores over A. MZI, B. CEI, C. NEI, D. NWI and E. SPI. Scores are calculated from (i)CFST126, (ii) CFST382 and (iii) GFSbc.

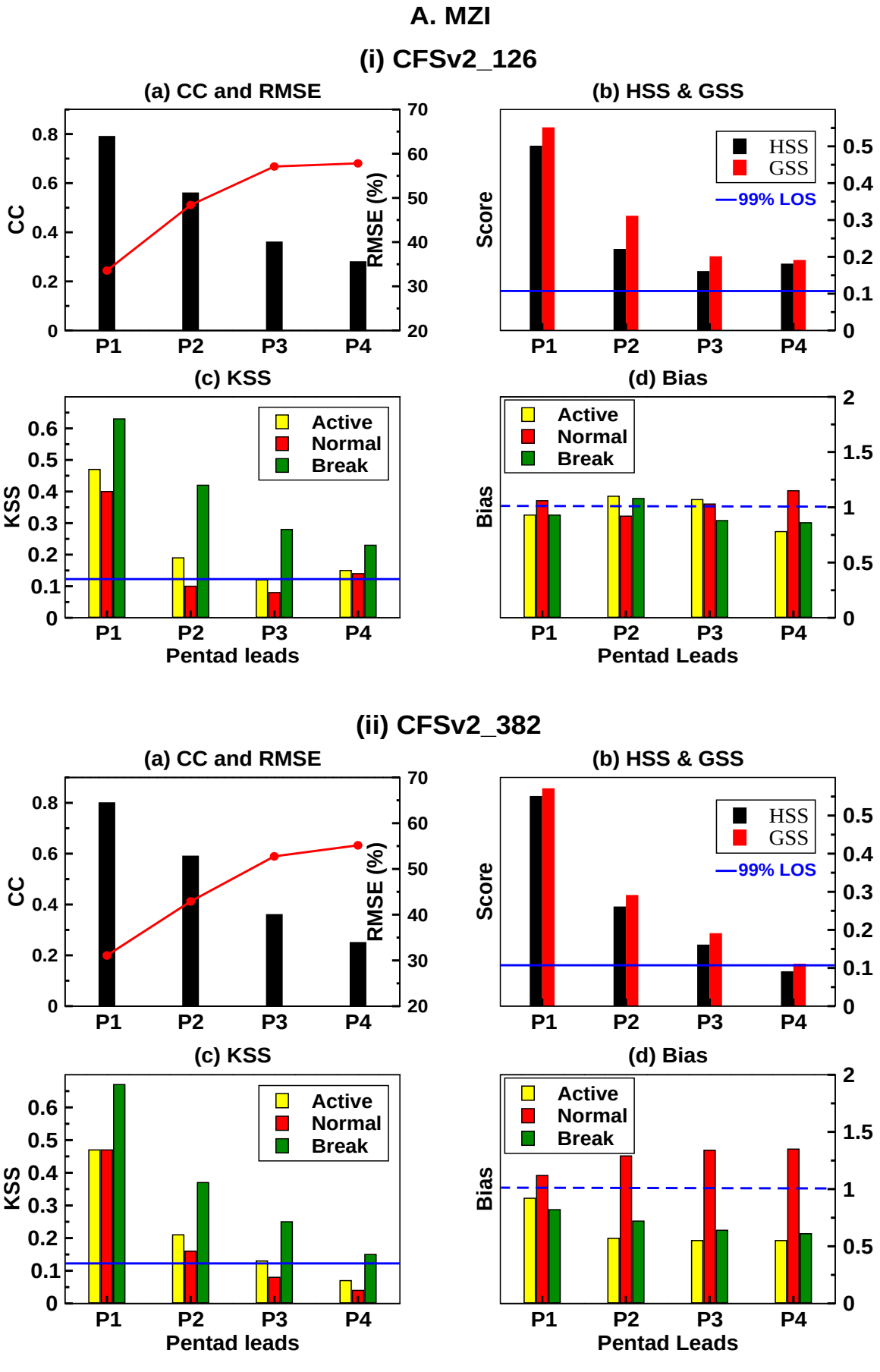

(iii) GFSbc

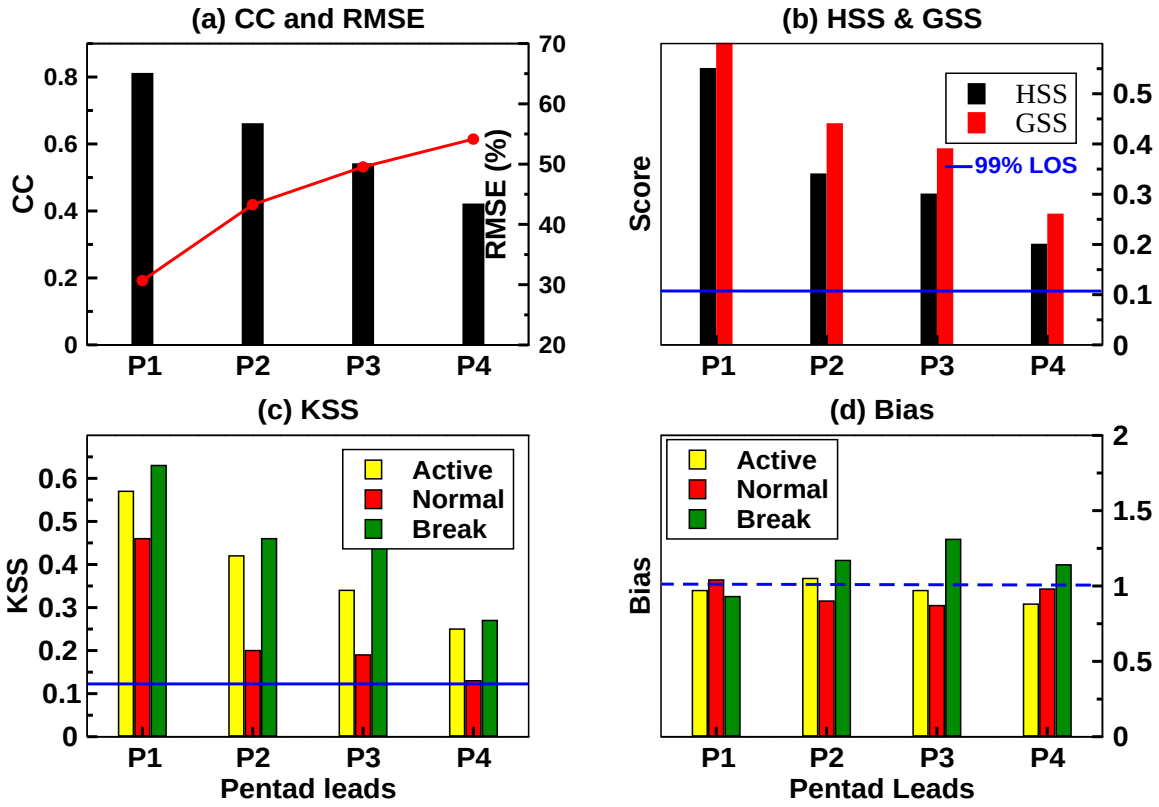

B. CEI

(i) CFSv2_126

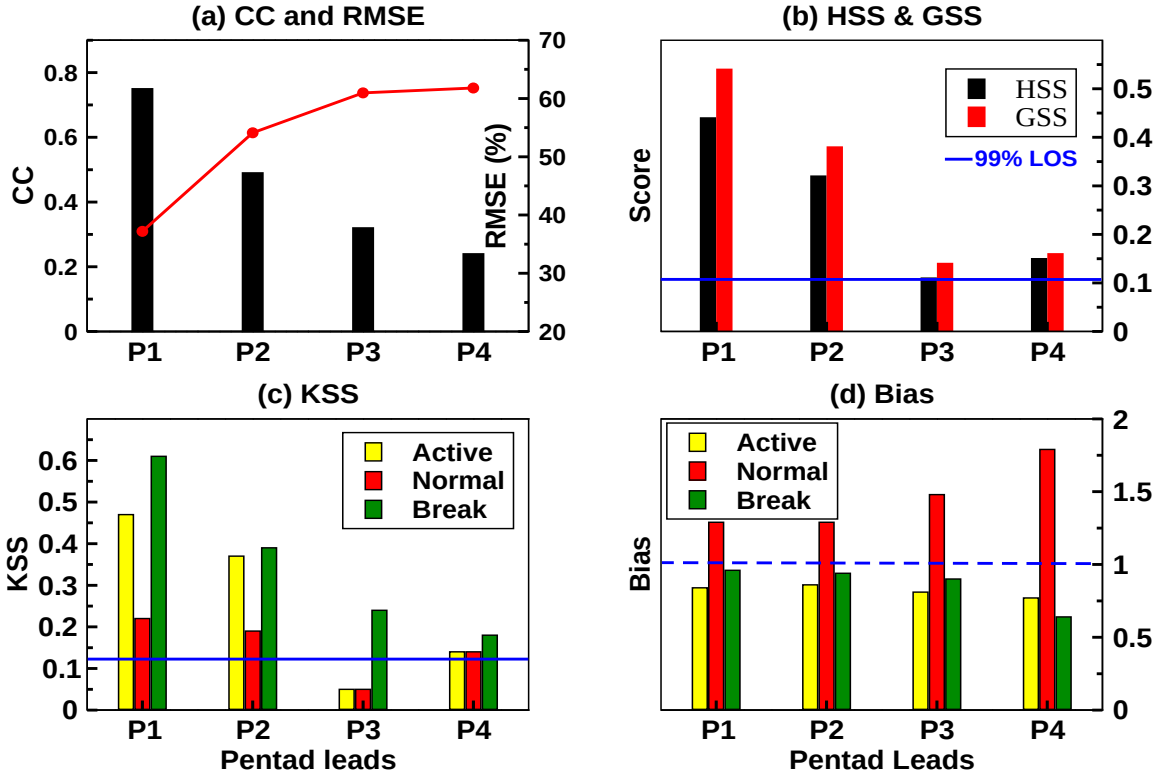

(ii) CFSv2_382

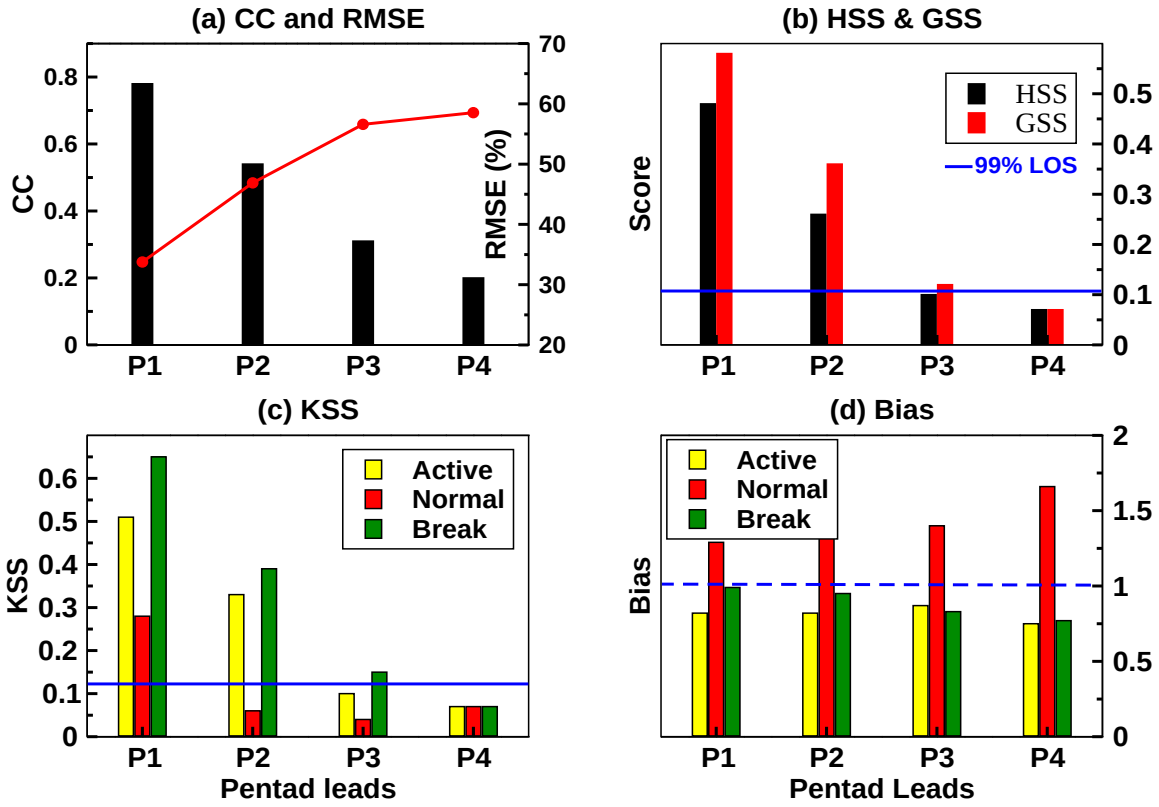

(iii) GFSbc

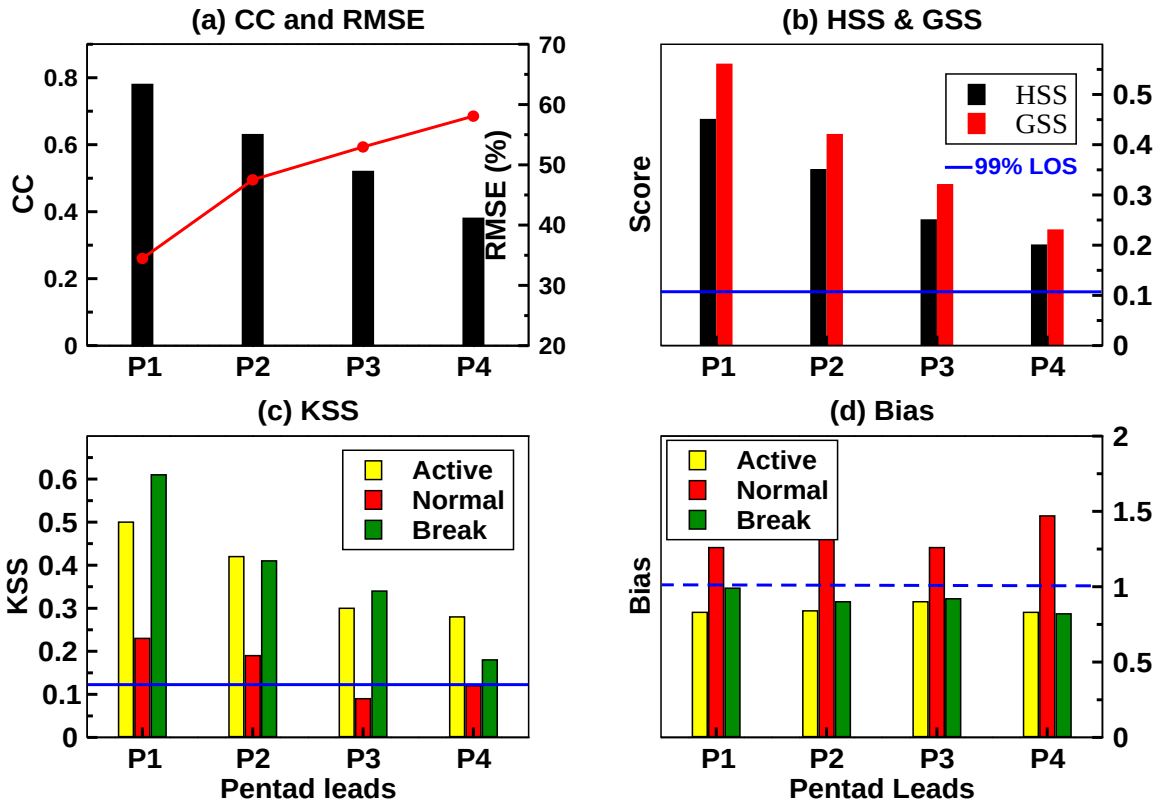

C. NEI

(i) CFSv2_126

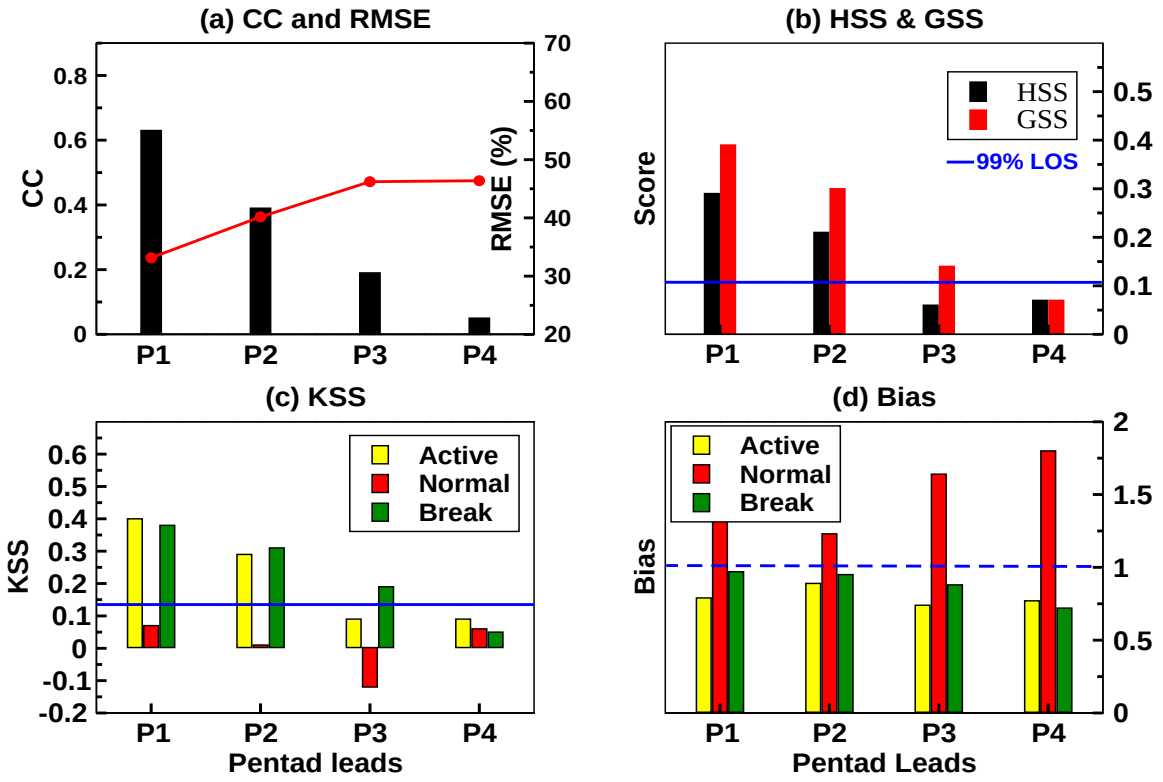

(ii) CFSv2_382

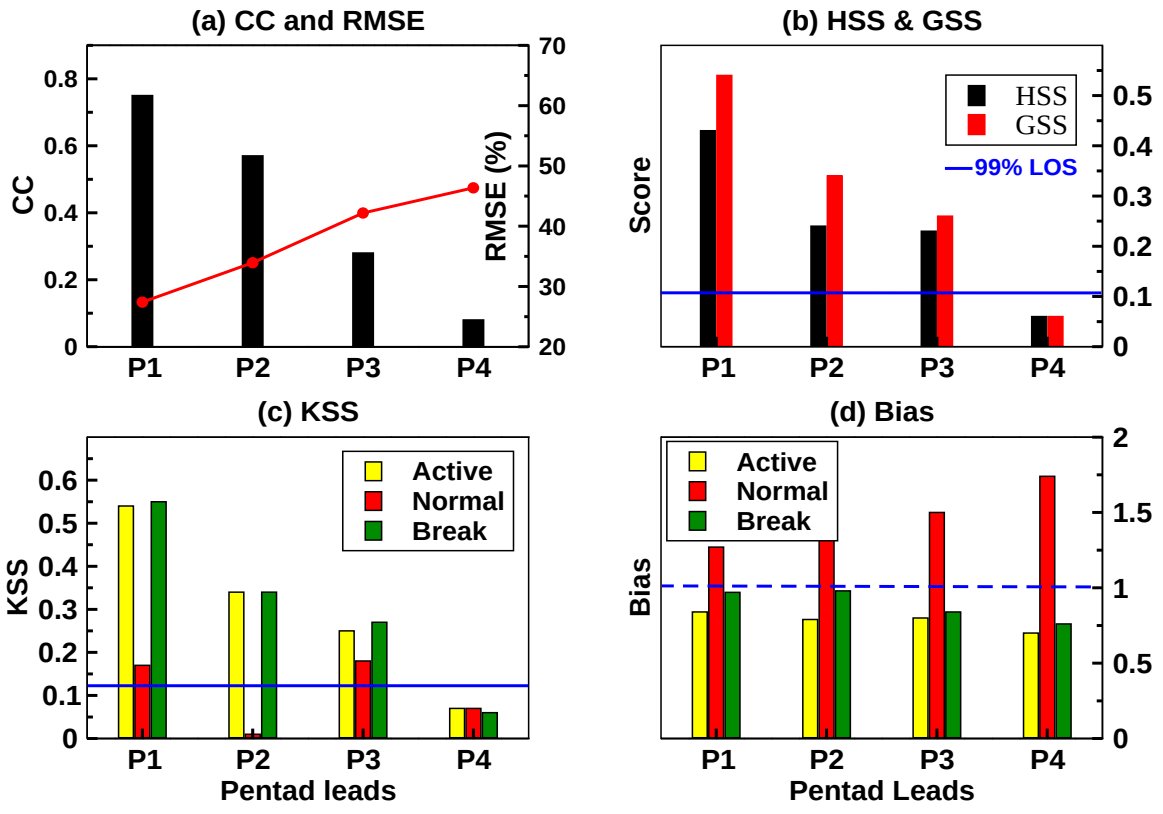

(iii) GFSbc

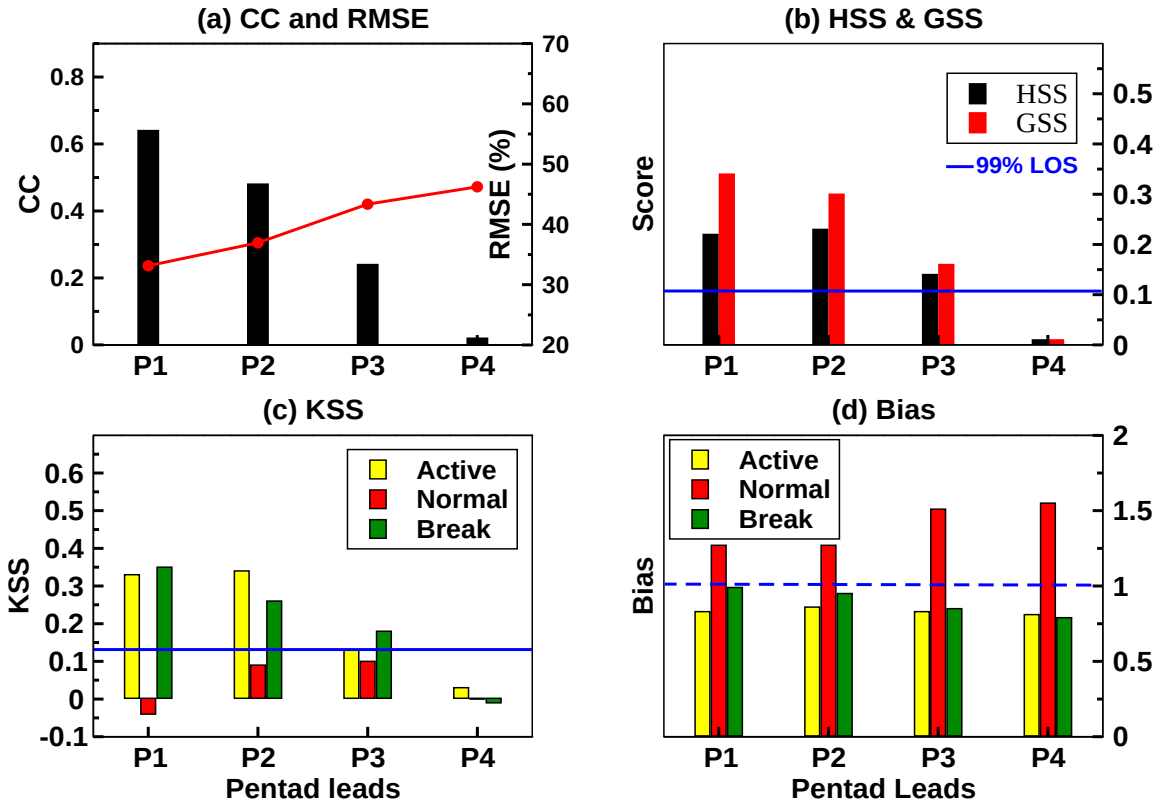

D. NWI

(i) CFSv2_126

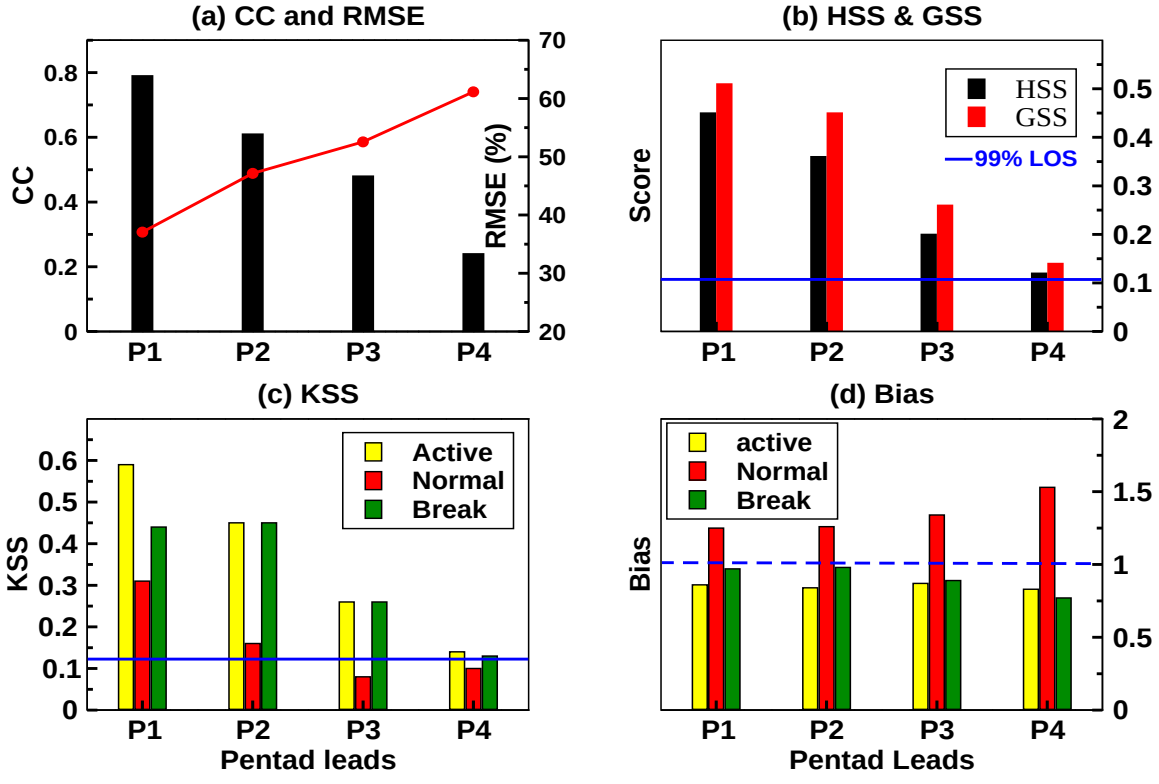

(ii) CFSv2_382

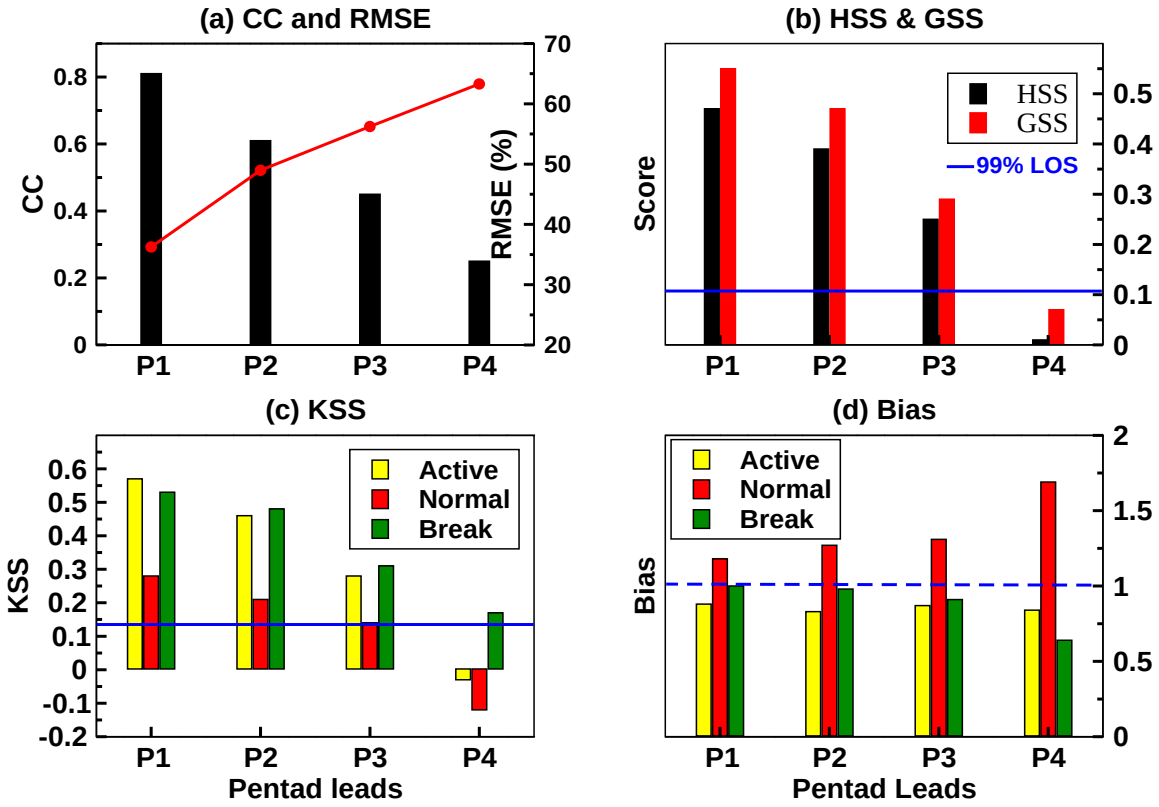

(iii) GFSbc

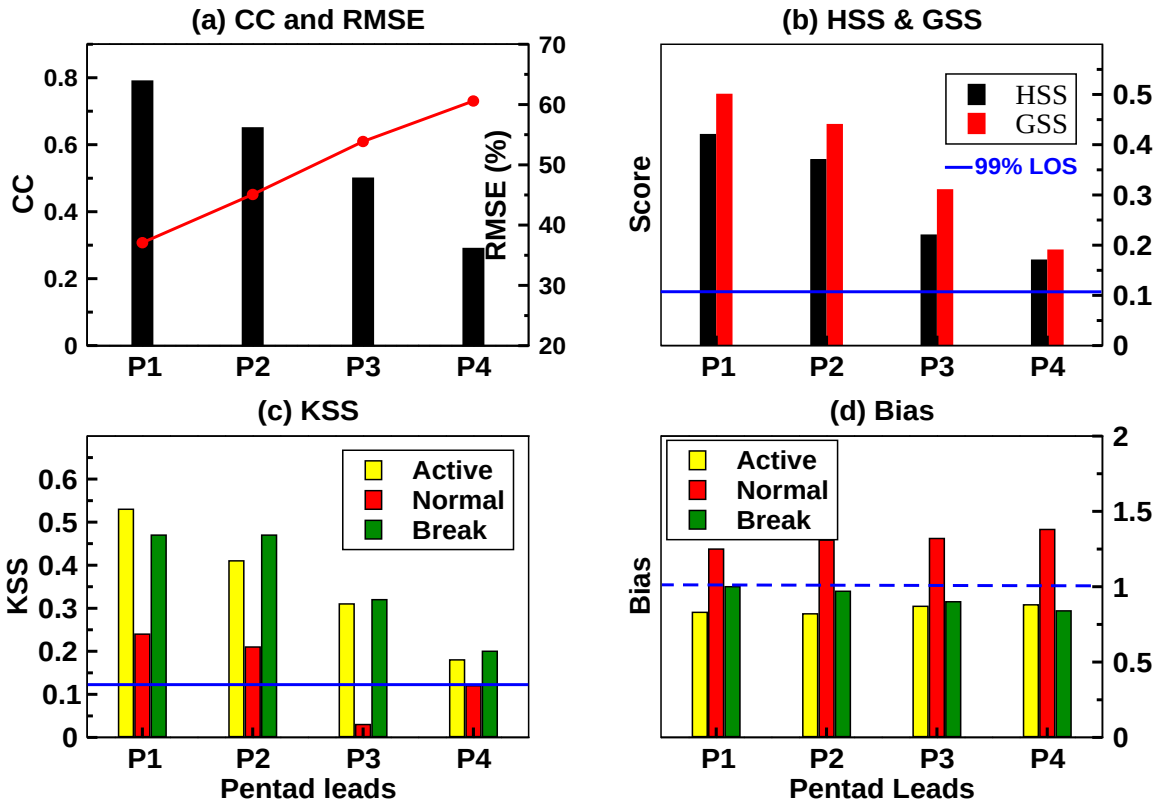

E. SPI

(ii) CFSv2_382

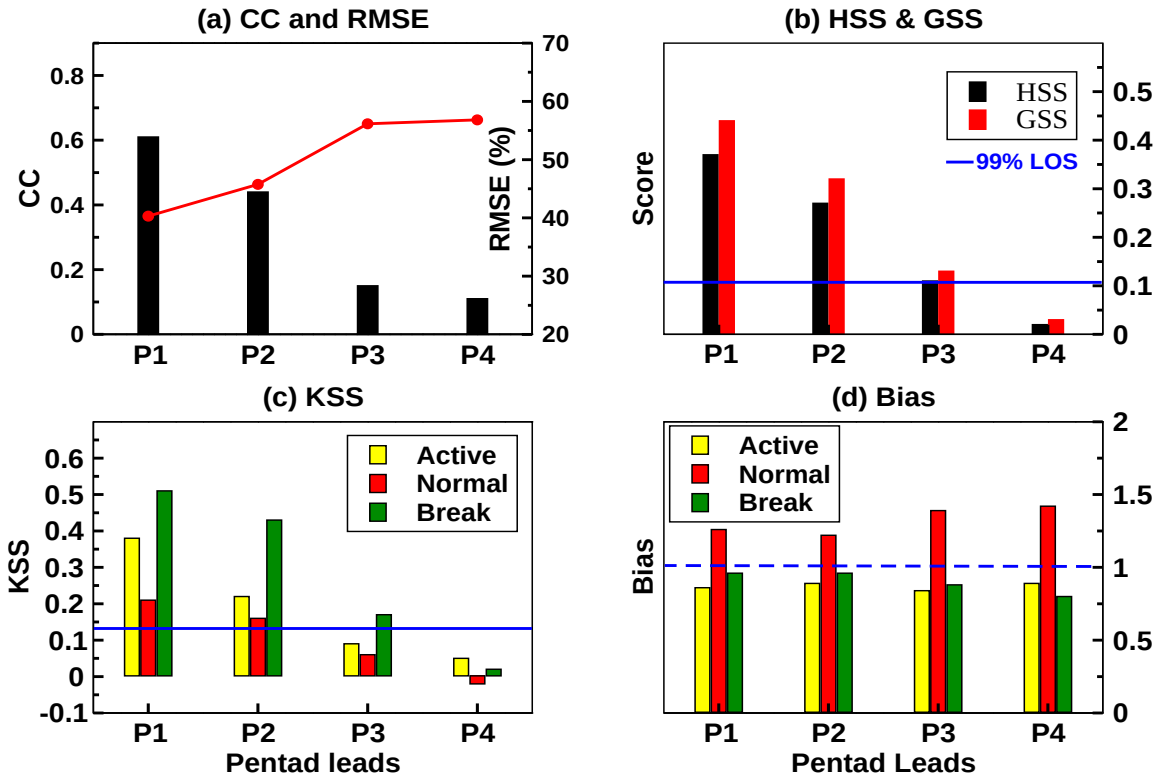

(ii) CFSv2_382

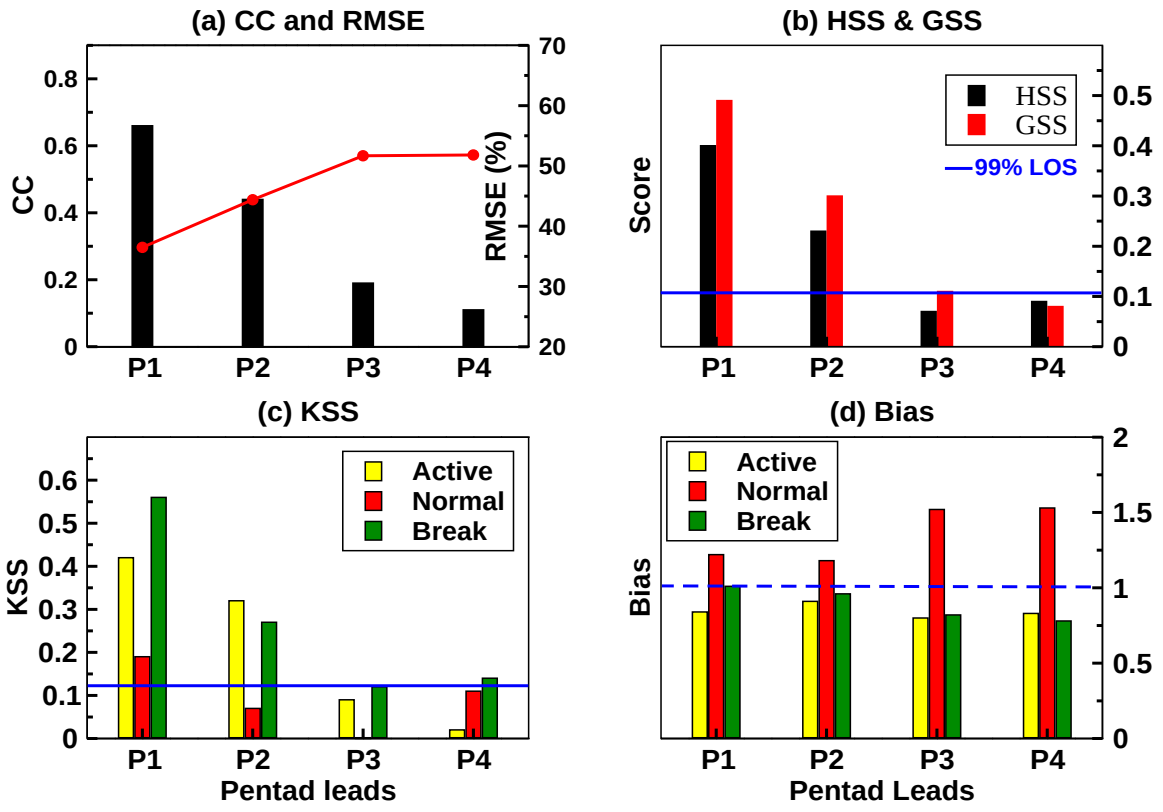

(iii) GFSbc

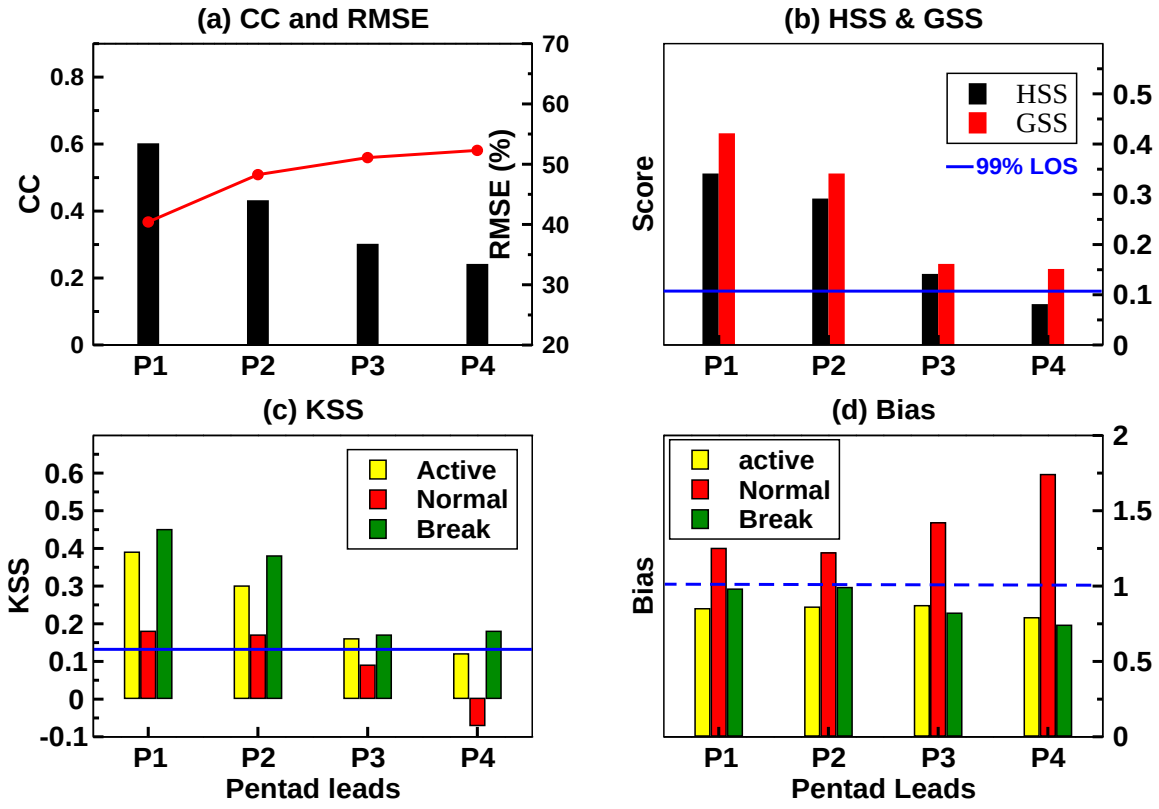
(a) CC and RMSE
CC
RMSE (%)
0
0.2
0.4
0.6
0.8
20
30
40
50
60
70
P1
P2
P3
P4
(b) HSS & GSS
Score
HSS
GSS
99% LOS
0
0.1
0.2
0.3
0.4
0.5
P1
P2
P3
P4
(c) KSS
KSS
Active
Normal
Break
-0.1
0
0.1
0.2
0.3
0.4
0.5
0.6
P1
P2
P3
P4
Pentad leads
(d) Bias
Bias
active
Normal
Break
0
0.5
1
1.5
2
P1
P2
P3
P4
Pentad Leads

Figure 14: ROC for CFST126, CFST382 and GFSbc for three categories [Above normal (AN), Near normal (NN) and Below normal (BN)] over A. CEI, B. NEI, C. NWI, D. SPI and E. MZI.

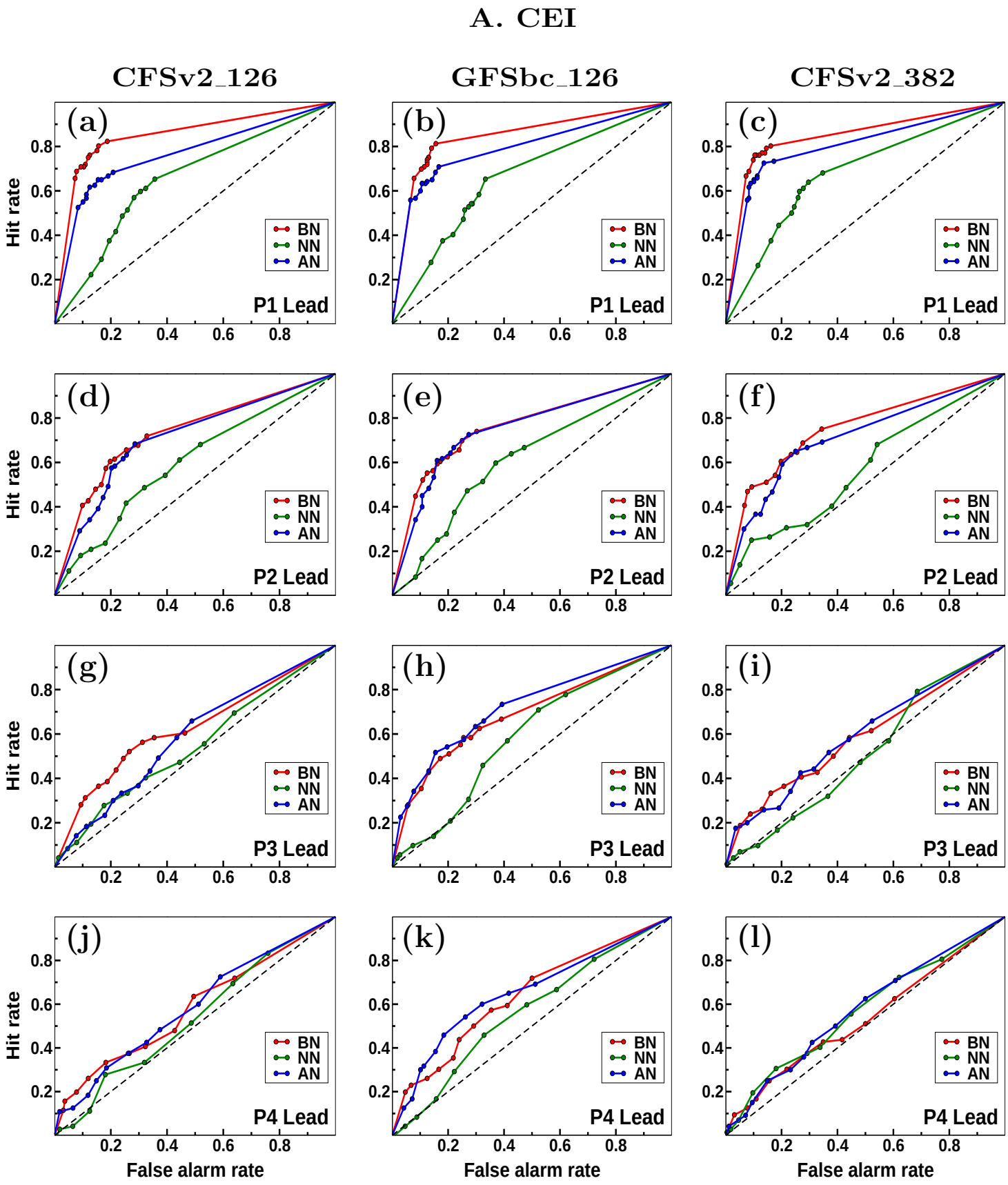

B. NEI

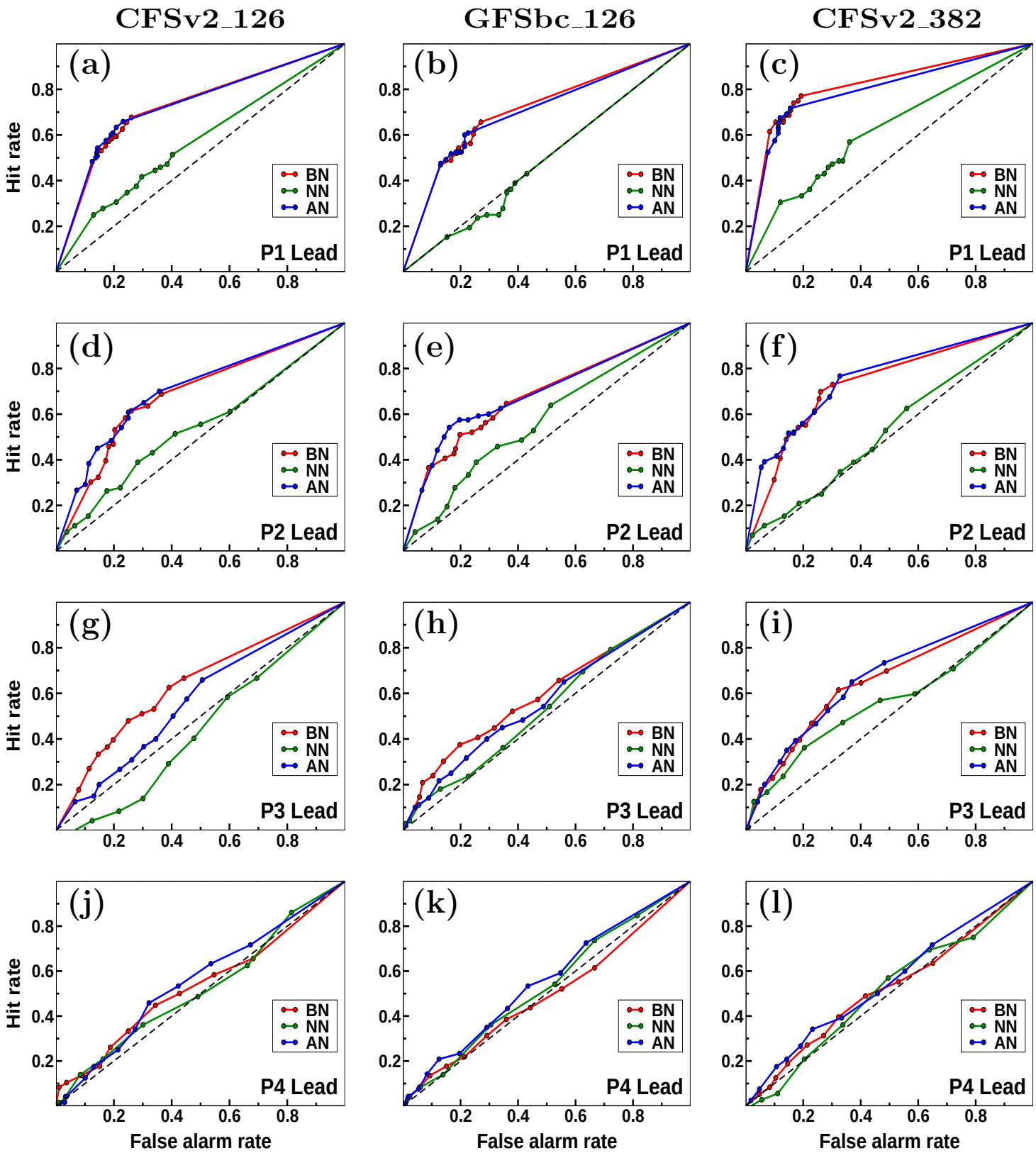
CFSv2_126
GFSbc_126
CFSv2_382
(a)
(b)
(c)
(d)
(e)
(f)
(g)
(h)
(i)
(j)
(k)
(l)
Hit rate
False alarm rate
BN
NN
AN
P1 Lead
P2 Lead
P3 Lead
P4 Lead
0.2
0.4
0.6
0.8

C. NWI

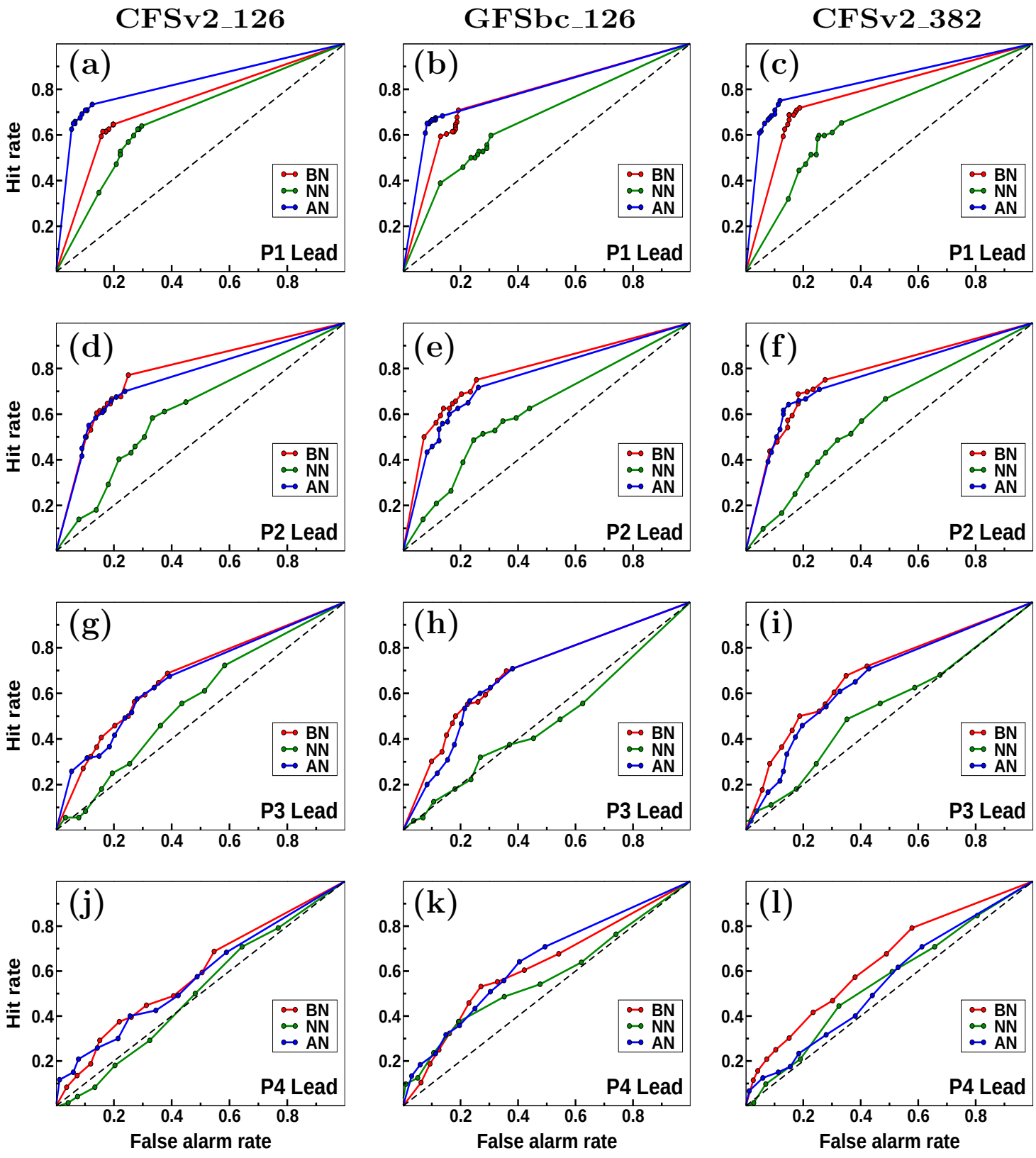
CFSv2_126
GFSbc_126
CFSv2_382
(a)
(b)
(c)
(d)
(e)
(f)
(g)
(h)
(i)
(j)
(k)
(l)
Hit rate
False alarm rate
BN
NN
AN
P1 Lead
P2 Lead
P3 Lead
P4 Lead
0.2
0.4
0.6
0.8

D. SPI

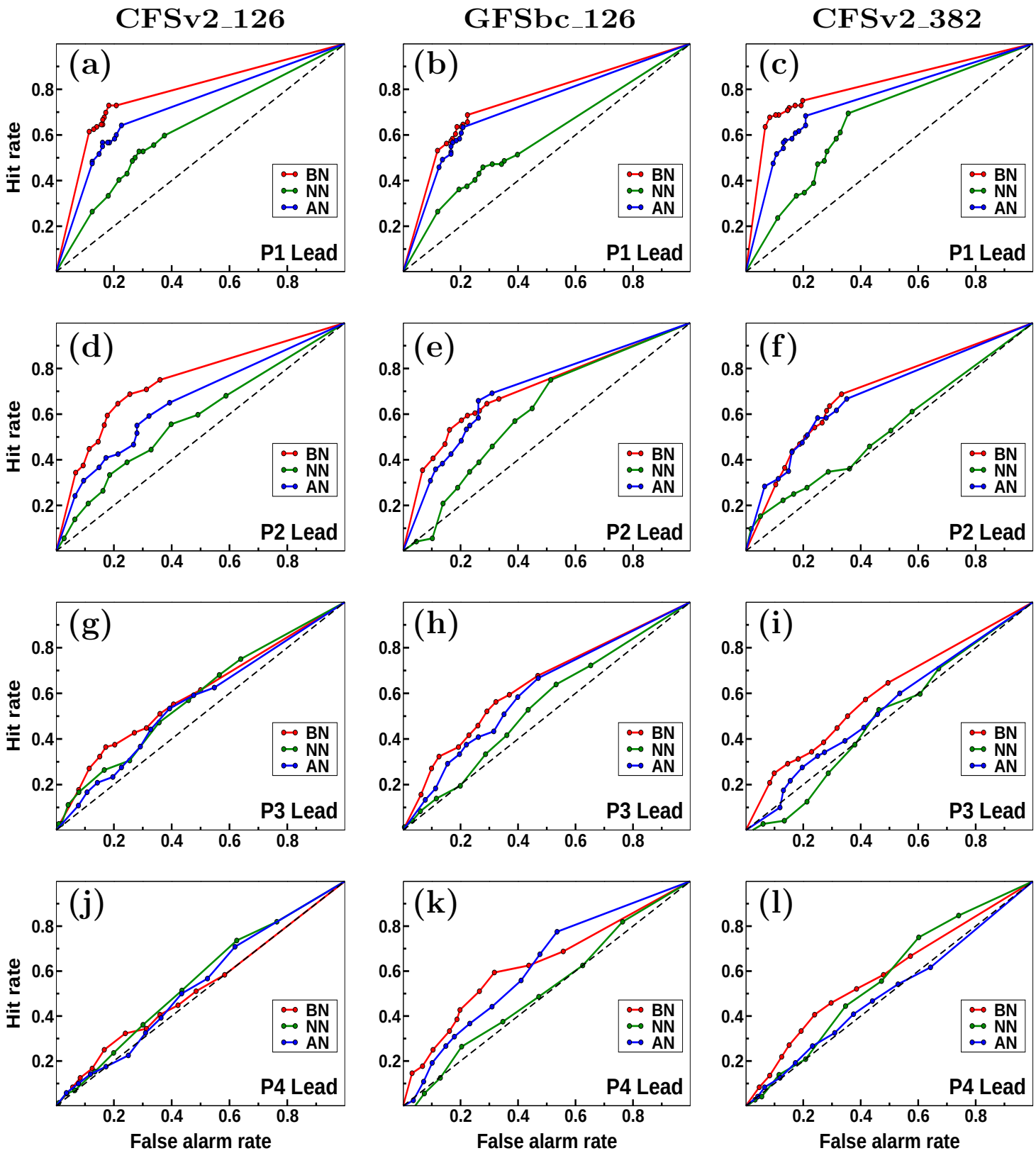
CFSv2_126
GFSbc_126
CFSv2_382
(a)
(b)
(c)
(d)
(e)
(f)
(g)
(h)
(i)
(j)
(k)
(l)
Hit rate
False alarm rate
BN
NN
AN
P1 Lead
P2 Lead
P3 Lead
P4 Lead
0.2
0.4
0.6
0.8

E. MZI

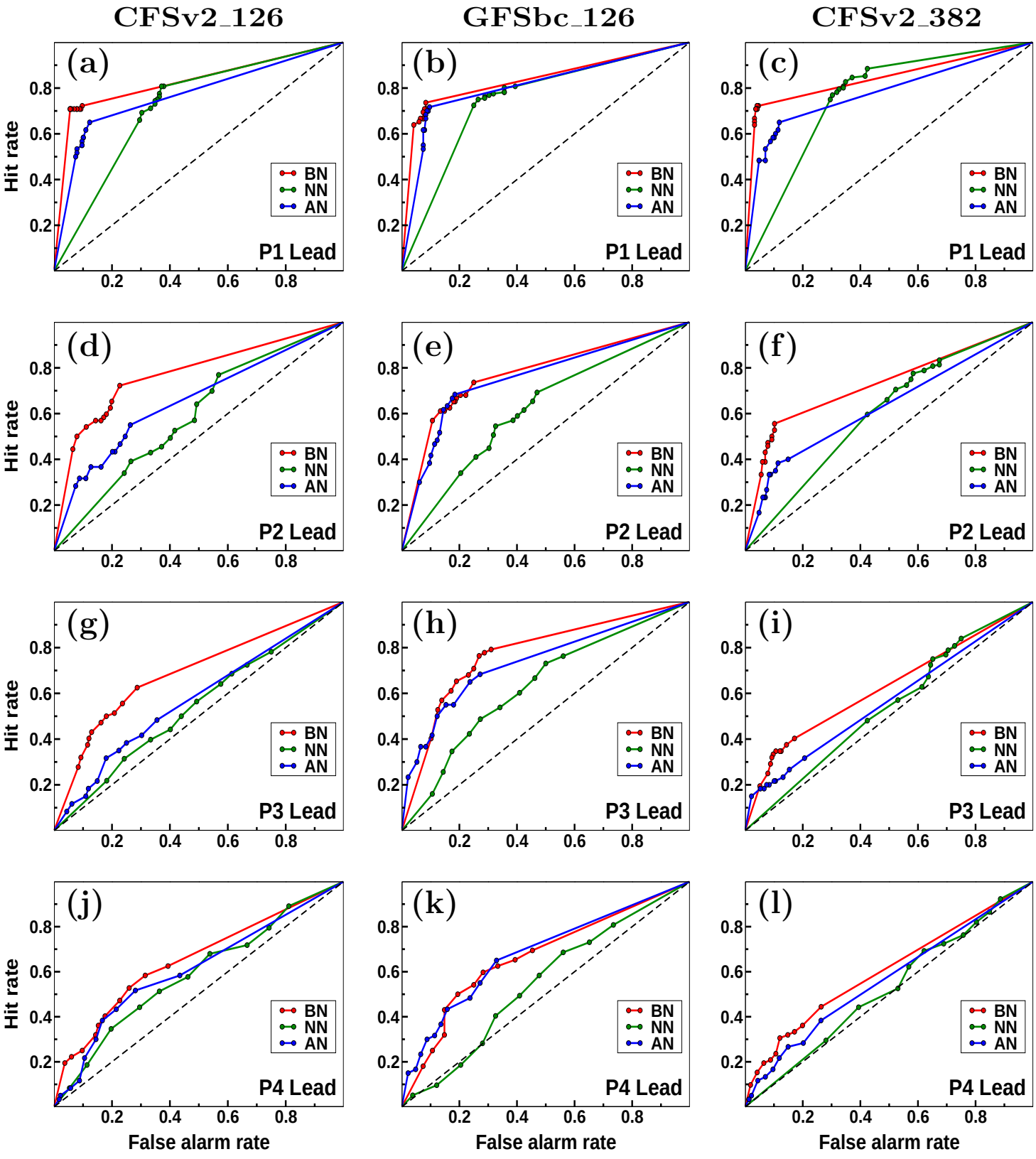
CFSv2_126
GFSbc_126
CFSv2_382
(a)
(b)
(c)
(d)
(e)
(f)
(g)
(h)
(i)
(j)
(k)
(l)
Hit rate
False alarm rate
BN
NN
AN
P1 Lead
P2 Lead
P3 Lead
P4 Lead
0.2
0.4
0.6
0.8

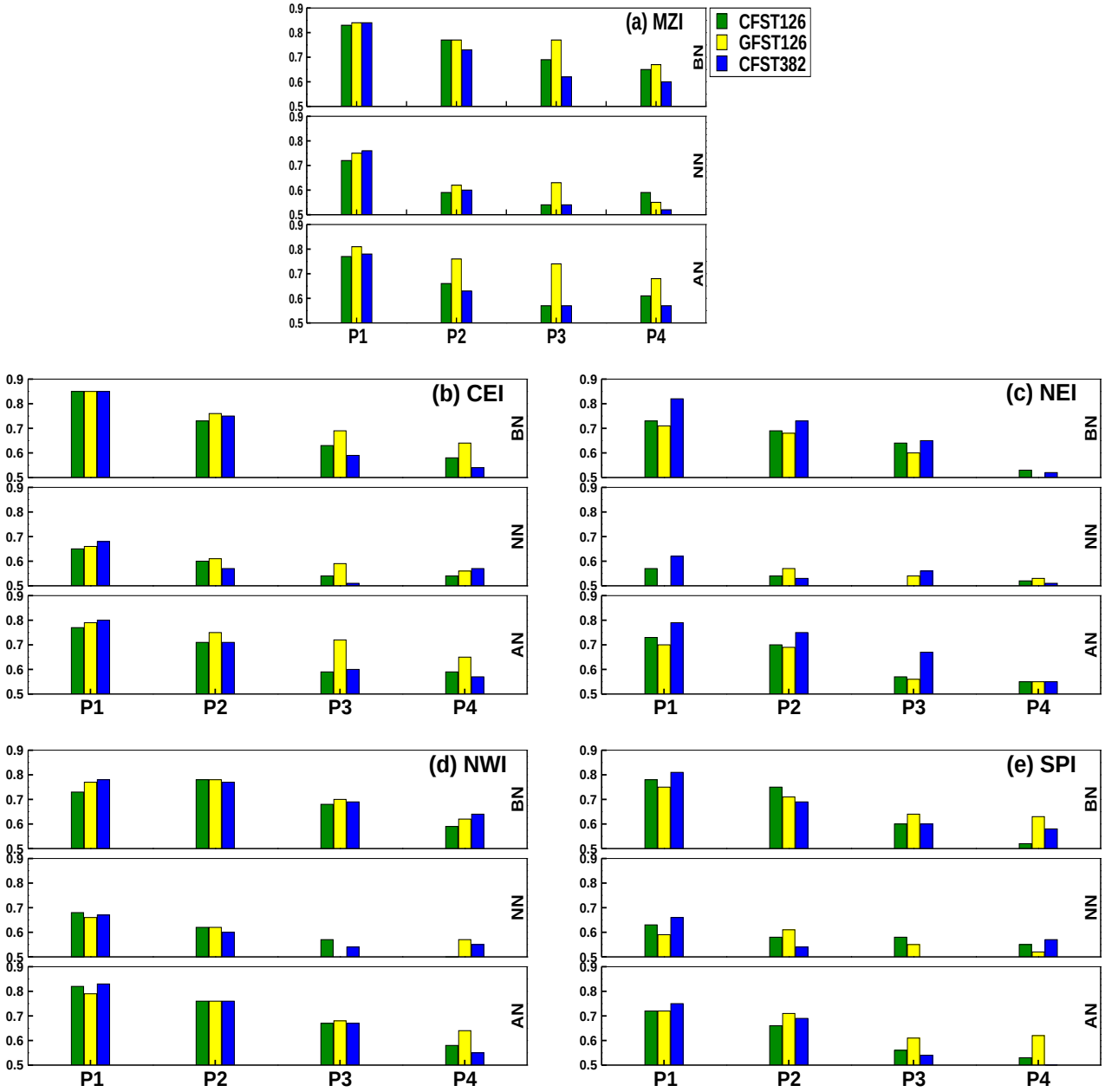

Figure 15: Area Under Curve (AUC) of ROC for CFST126, CFST382 and GFSbc for three categories [Above normal (AN), Near normal (NN) and Below normal (BN)] over MZI, CEI, NEI, NWI and SPI.

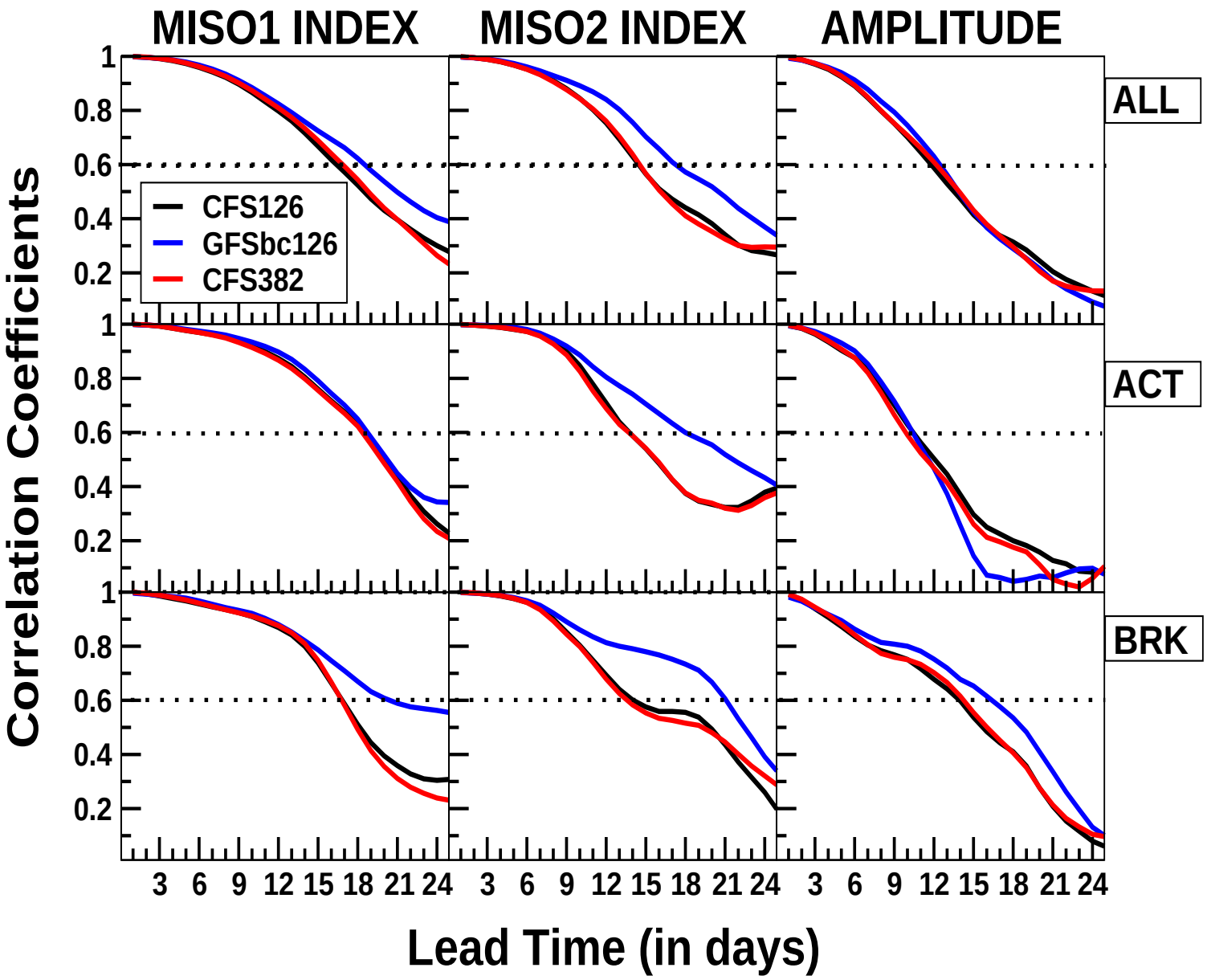

Figure 16: Pentad lead prediction skill of large scale MISO1 index (left panel), MISO2 index (middle panel) and Amplitude (right panel) from All start dates (top panel), Active start dates (middle panel) and Break start dates (bottom panel).